IMPLICIT-EXPLICIT METHODS FOR DIFFUSIVELY CORRECTED MULTI-SPECIES KINEMATIC FLOW MODELS

RAIMUND BÜRGER*, PEP MULET†, AND LUIS M. VILLADA‡

Abstract. Implicit-explicit methods are a suitable choice for the solution of nonlinear convection-diffusion equations, since the stability restrictions, coming from the explicitly treated convective part, are much less severe than those that would be deduced from an explicit treatment of the diffusive term. These schemes usually combine an explicit Runge-Kutta scheme for the time integration of the convective part with a diagonally implicit one for the diffusive part. The application of these schemes to multi-species kinematic flow models with strongly degenerate diffusive corrections requires the solution of highly nonlinear and non-smooth systems of algebraic equations. Since the efficient solution of these systems by the Newton-Raphson method requires some degree of smoothness, it is proposed to regularize the diffusion coefficients in the model and to apply suitable techniques to solve these nonlinear systems in an efficient way. Numerical examples arising from models of polydisperse sedimentation and multi-class traffic flow confirm the efficiency of the methods proposed.

Key words. Kinematic flow models, degenerate convection-diffusion equations, implicit-explicit Runge-Kutta schemes, polydisperse sedimentation, multi-class traffic models, hyperbolicity.

AMS subject classifications. 35L40, 35L65, 35M33, 65M06, 76T20.

1. Introduction.

1.1. Scope. Multi-species kinematic flow models arise in many engineering applications that involve the flow of one disperse substance through a continuous phase, and where the disperse substance consists of particles belonging to a number N of species that can be distinguished by some characteristic property. These species usually segregate with respect to a distinguished spatial direction (for instance, that of gravity or another applied body force) and form areas of different composition. Examples are the settling of particles differing in size or density in a polydisperse solid-liquid suspension [5] and multi-class traffic models [4, 42]. The term "kinematic" means that the velocity v_i of species i is an explicit function of the vector $\Phi = (\phi_1, \ldots, \phi_N)^{\mathrm{T}} \in \mathbb{R}^N$ of the concentrations (volume fractions) ϕ_i of each species. Thus, standard multi-species kinematic flow models are given by systems of N scalar, in general nonlinear first-order conservation laws

$$\partial_t \Phi + \partial_x \boldsymbol{f}(\Phi) = \mathbf{0}, \quad \boldsymbol{f}(\Phi) = (f_1(\Phi), \ldots, f_N(\Phi))^{\mathrm{T}} = \big(\phi_1 v_1(\Phi), \ldots, \phi_N v_N(\Phi)\big)^{\mathrm{T}}, \tag{1.1}$$

where t is time and x is the spatial coordinate. In this work we focus on numerical methods for multi-species flow models in which the velocities also depend on the spatial variation of Φ to account for additional effects such as sediment compressibility or drivers' reaction time and anticipation length in traffic flow. These corrections can be usually posed in such a way that the resulting system of partial differential equations (PDEs) has an extra, possibly strongly degenerate diffusive term. We therefore

*CI^{2}MA and Departamento de Ingeniería Matemática, Facultad de Ciencias Físicas y Matemáticas, Universidad de Concepción, Casilla 160-C, Concepción, Chile. E-Mail: rburger@ing-mat.udec.cl

†Departament de Matemàtica Aplicada, Universitat de València, Av. Dr. Moliner 50, E-46100 Burjassot, Spain. E-Mail: mulet@uv.es

‡CI^{2}MA and Departamento de Ingeniería Matemática, Facultad de Ciencias Físicas y Matemáticas, Universidad de Concepción, Casilla 160-C, Concepción, Chile. E-Mail: lmvillada@ing-mat.udec.cl

consider systems of PDEs of the type

$$\partial_t \Phi + \partial_x \boldsymbol{f}(\Phi) = \partial_x \big(\boldsymbol{B}(\Phi) \partial_x \Phi \big), \tag{1.2}$$

where $\boldsymbol{B}(\Phi)$ is a given $N \times N$ matrix function expressing the diffusive correction. The system (1.2) is supplied with an initial condition and, depending on the application, zero-flux or periodic boundary conditions.

Although the available mathematical theory does not allow us to be conclusive about the existence, uniqueness and well-posedness of the solutions of such strongly degenerate hyperbolic-parabolic systems, it is plausible to perform simulations with appropriate numerical methods. Explicit schemes for hyperbolic systems of first-order conservation laws are widely used in many applications nowadays. Although they can be rather slow for some steady state computations, due to CFL stability restrictions on the time step size, their use for unsteady computations is deemed as practical in many situations. This does not hold when diffusion terms are present. However, one can resort to an implicit treatment of these terms to overcome the drastic step size restrictions imposed by the stability of explicit schemes applied to parabolic equations.

It is the purpose of the present work to demonstrate the benefits of using implicit-explicit (IMEX) schemes for the efficient solution of initial-boundary value problems for (1.2) under specific assumptions of diffusively corrected kinematic flow models. These specific properties, which are reflected in the design of the numerical schemes and in our analysis, include that the number N of species (and therefore of scalar equations) may be arbitrarily large; that the flux vector $\boldsymbol{f}(\Phi)$ is constructed in a systematic way that makes characteristic-wise schemes applicable (even though the eigenstructure of the flux Jacobian $\mathcal{J}_{\boldsymbol{f}}(\Phi)$ is not available in closed algebraic form); and that (1.2) is often strongly degenerate, where the location of the type-change interface is unknown beforehand, and $\boldsymbol{B}$ may even be discontinuous as a function of Φ. We focus on a model of sedimentation of polydisperse suspensions forming compressible sediment layers, and a diffusively corrected multi-class Lighthill-Whitham-Richards (LWR) model for vehicular traffic that includes anticipation length and reaction time.

The main novelty of this work is the particular method of solution of the nonlinear systems that appear with the implicit treatment of the degenerate diffusion term. This method consists in the Newton-Raphson method applied after regularizing the non-smooth diffusion coefficient. The final schemes are much more efficient, in term of error reduction versus CPU time, than the explicit schemes.

1.2. Related work. First-order models of the type (1.1) have been widely studied in recent years, with an emphasis on polydisperse sedimentation [5, 8, 9, 18, 43] and multiclass vehicular traffic [4, 16, 32, 42, 45, 46, 47]. Other applications include the settling and creaming of emulsions and dispersions [19, 37] (these lists of references are incomplete). Among the polydisperse sedimentation models, one of the most widely used velocity model is the Masliyah-Lockett-Bassoon (MLB) model [27, 28]. We refer to [8, 44] for alternate velocity models. On the other hand, the multi-class extension of the LWR model [25, 35], the MCLWR model, was introduced by Benzoni-Gavage and Colombo [4] and Wong and Wong [42]. All these models have in common that although the functions v_i are constructed in a systematic manner, the eigenvectors and eigenvalues of the Jacobian $\mathcal{J}_{\boldsymbol{f}}(\Phi) = (\partial f_i(\Phi)/\partial \phi_j)_{1 \le i,j \le N}$ are usually not available in closed algebraic form. It is in general difficult to estimate the subregion of N-dimensional phase space where the model (1.1) is strictly hyperbolic, i.e., $\mathcal{J}_{\boldsymbol{f}}(\Phi)$ has pairwise distinct real eigenvalues, or to solve the Riemann problem for (1.1) exactly or approximately. However, for some of these models, the functions v_i

depend on a small number of independent scalar functions of Φ only, so that $\mathcal{J}_{\boldsymbol{f}}(\Phi)$ is a low-rank perturbation of a diagonal matrix. In this case, the calculus of the so-called secular equation, advanced first by Anderson [2], allows one to establish that, under determined circumstances, the eigenvalues of $\mathcal{J}_{\boldsymbol{f}}(\Phi)$ are real and interlace with the velocities v_i [8, 17]. This information provides starting values to determine the exact eigenvalues by a root finder, and eventually to determine the corresponding eigenvectors. This has led to the construction of involved but efficient characteristic-wise weighted essentially non-oscillatory (WENO) schemes [23, 26, 38, 39] for (1.1) [9, 16]. These schemes are employed herein to discretize the convective part of (1.2).

For models of polydisperse sedimentation, diffusive terms leading to the form (1.2) were first proposed by Stamatakis and Tien [41]. A theory of sedimentation of polydisperse suspensions forming compressible sediments was advanced in [5], where the system (1.2) was solved by the Kurganov-Tadmor (KT) explicit high-resolution central difference scheme [24]. Its application to strongly degenerate convection-diffusion systems is explicitly proposed in [24, Sect. 4.2]. On the other hand, the multi-class version of the diffusively corrected LWR model proposed by Nelson [30], which can also be understood as a diffusively corrected version of the MCLWR traffic model [4, 42], is newly derived herein. We also mention that in a very recent paper, Abeynaike et al. [1] propose a model for the sedimentation and creaming of size-distributed droplets in glycerol/biodiesel dispersions that is equivalent to (1.2).

An IMEX Runge-Kutta scheme consists in applying a Runge-Kutta scheme with an implicit discretization of the diffusive term and an explicit one for the convective term. To introduce the main idea, we consider the problem

$$\partial_t \boldsymbol{\Phi} = C(\boldsymbol{\Phi}) + D(\boldsymbol{\Phi}), \tag{1.3}$$

where $C(\boldsymbol{\Phi})$ and $D(\boldsymbol{\Phi})$ are discretizations of the convective and diffusive terms, respectively. The stability restriction on the time step Δt that explicit schemes impose when applied to (1.3) is very severe (Δt must be proportional to the square Δx^2 of the grid spacing), due to the presence of $D(\boldsymbol{\Phi})$. The implicit treatment of both $C(\boldsymbol{\Phi})$ and $D(\boldsymbol{\Phi})$ would remove any stability restriction on Δt, but the upwind nonlinear discretization of $C(\boldsymbol{\Phi})$ that is needed for stability makes its implicit treatment extremely involved. In fact, after the pioneering work of Crouzeix [11], numerical integrators that deal implicitly with $D(\boldsymbol{\Phi})$ and explicitly with $C(\boldsymbol{\Phi})$ can be used with a time step restriction dictated by the convective term alone. These schemes, apart of having been profusely used in convection-diffusion problems and convection problems with stiff reaction terms (see [3, 15] and references therein), have been recently used to deal with stiff terms in hyperbolic systems with relaxation (see [6, 7, 34]).

1.3. Outline of the paper. The remainder of the paper is organized as follows. In Section 2 we introduce the diffusively corrected multi-species kinematic flow models chosen for numerical simulation, namely the model of polydisperse suspensions forming compressible sediments (cf. [5]) and the multi-class version of the diffusively corrected LWR traffic model (cf. [30]) (see Section 1.2). The results of the hyperbolicity analysis (cf. [8, 17]) of the non-diffusive versions (1.1) of both models are summarized, and the structure of the respective diffusion term is analyzed. The numerical schemes to solve (1.2) are introduced in Section 3, starting with a semi-discrete formulation (Section 3.1) in which the spatial derivatives are discretized. The convective terms are discretized by the spectral WENO schemes for (1.1) introduced in [9, 16]. The discretization of the zero-flux and periodic boundary conditions (for the polydisperse sedimentation and multi-class traffic models, respectively) is specified in Section 3.2.

After briefly commenting on explicit fully-discrete schemes (in Section 3.3), we describe in Section 3.4 the fully discrete implicit-explicit schemes studied herein. The time discretization by IMEX-RK schemes is outlined in Section 3.5. The implementation of these schemes requires the solution of nonlinear systems of algebraic equations in each time step. The numerical solution of these nonlinear systems is addressed in Section 4, in which two solvers are described, namely a simple fixed-point (FP) iteration (Section 4.1) and a Newton-Raphson (NR) method (Section 4.2). The latter is at the core of this paper, and incorporates a line-search strategy combined with a regularization $\boldsymbol{B}_\varepsilon(\Phi)$ of the terms coming from the possibly discontinuous behaviour of $\boldsymbol{B}(\Phi)$, where the regularization parameter ε is successively reduced during the NR method. In Section 5 numerical results are presented for four examples, namely for the polydisperse sedimentation model with $N = 3$ and $N = 8$ (Examples 1 and 2, Sections 5.1 and 5.2) and for the diffusively corrected MCLWR model with $N = 3$ (Examples 3 and 4 with different initial densities, see Section 5.3). Numerical results indicate that IMEX-RK schemes based on formulas with at least two non-trivial stages are significantly more efficient in reducing numerical error than the explicit KT scheme, and that whenever $\boldsymbol{B}(\Phi)$ is smooth and both the FP and NR nonlinear solvers are applicable, the latter is more efficient. These and other conclusions are summarized in Section 6.

2. Diffusively corrected multi-species kinematic flow models.

2.1. Polydisperse sedimentation. We consider a model of sedimentation of a suspension of equal-density particles, which are assumed to belong to N species with sizes $d_1 > d_2 > \cdots > d_N$. We let ϕ_i denote the local volume fraction of species i having size d_i, and define $\phi := \phi_1 + \cdots + \phi_N$. The evolution of $\Phi = \Phi(x,t)$ as a function of depth x and time t in a one-dimensional column is then governed by the combined effects of hindered settling and sediment compressibility. These effects determine the convective and diffusive parts, respectively, of the following system of convection-diffusion equations (see [5]):

$$\partial_t \phi_i + \partial_x f_i(\Phi) = \partial_x\big(a_i(\Phi, \partial_x \Phi)\big), \quad i = 1, \ldots, N, \quad 0 < x < K, \quad t > 0, \tag{2.1}$$

which is supplemented by the initial condition $\Phi(x,0) = \Phi_0(x)$ for $0 \le x \le K$, where Φ_0 is the given initial concentration distribution, and zero-flux boundary conditions corresponding to settling in a closed column of height K, i.e.,

$$\phi_i v_i = f_i(\Phi) - a_i(\Phi, \partial_x \Phi) = 0 \quad \text{for } x = 0 \text{ and } x = K, \quad t > 0. \tag{2.2}$$

Here the flux density functions $f_1, \ldots, f_N$ are those of the MLB model given by

$$f_i(\Phi) = \mu \bar{\varrho}_{\mathrm{s}} \phi_i V(\phi)(1-\phi)(\delta_i - \boldsymbol{\delta}^T \Phi), \quad i = 1, \ldots, N, \tag{2.3}$$

where $\mu > 0$ is a viscosity constant, $\bar{\varrho}_{\mathrm{s}} > 0$ is the solid mass density minus the fluid density, $\delta_i := d_i^2/d_1^2$, $\boldsymbol{\delta} := (\delta_1 = 1, \delta_2, \ldots, \delta_N)^{\mathrm{T}}$, and $V(\phi)$ is a hindered settling function that is assumed to satisfy $V(\phi) \ge 0$ for all ϕ, $V(0) = 1$ and $V'(\phi) < 0$. A typical expression due to Richardson and Zaki [36] is given by

$$V(\phi) = \begin{cases} (1-\phi)^{n_{\mathrm{RZ}}-2} & \text{for } 0 \le \phi \le \phi_{\max}, \\ 0 & \text{otherwise.} \end{cases} \tag{2.4}$$

The diffusion functions on the right-hand side of (2.1) are given by

$$a_i(\Phi, \partial_x \Phi) = \alpha_{i,1}(\Phi)\partial_x \phi_1 + \cdots + \alpha_{N,1}(\Phi)\partial_x \phi_N, \quad i = 1, \ldots, N, \tag{2.5}$$

where

$$\alpha_{ij} := \frac{\mu V(\phi)}{g\phi}\Big\{(1-\phi)\phi_i(\delta_i - \boldsymbol{\delta}^{\mathrm{T}}\Phi)\sigma_{\mathrm{e}}'(\phi) \\ - \left[\delta_i\delta_{ij} - \delta_j\phi_i - \frac{\phi_i}{\phi}(\delta_i - \boldsymbol{\delta}^{\mathrm{T}}\Phi)\right]\sigma_{\mathrm{e}}(\phi)\Big\}, \quad i,j = 1,\dots,N, \tag{2.6}$$

where δ_{ij} is the standard Kronecker symbol. Here σ_{e} denotes the effective solid stress function, and σ_{e}' is its derivative. This function is assumed to satisfy

$$\sigma_{\mathrm{e}}(\phi), \sigma_{\mathrm{e}}'(\phi) \begin{cases} = 0 & \text{for } \phi \le \phi_{\mathrm{c}}, \\ > 0 & \text{for } \phi > \phi_{\mathrm{c}}, \end{cases} \tag{2.7}$$

where ϕ_{c} is a critical concentration at which the particles touch each other. A typical function σ_{e} having these properties is given by

$$\sigma_{\mathrm{e}}(\phi) = \begin{cases} 0 & \text{for } \phi \le \phi_{\mathrm{c}}, \\ \sigma_0\big((\phi/\phi_{\mathrm{c}})^k - 1\big) & \text{for } \phi > \phi_{\mathrm{c}}, \end{cases} \quad \sigma_0, k > 0. \tag{2.8}$$

Defining the matrix $\boldsymbol{B}(\Phi) := (\alpha_{ij})_{1\le i,j\le N}$ and $\boldsymbol{f}(\Phi) = (f_1(\Phi),\dots,f_N(\Phi))$ we can rewrite (2.1) in the form (1.2).

2.2. Hyperbolicity and parabolicity analysis for the polydisperse sedimentation model. For the flux (2.3), $\mathcal{J}_{\boldsymbol{f}}(\Phi)$ is a rank-two perturbation of a diagonal matrix. This property allows one to analyze hyperbolicity, to localize eigenvalues, and to eventually calculate the corresponding eigenvectors of $\mathcal{J}_{\boldsymbol{f}}(\Phi)$, by using the so-called secular equation [2], see [8, 17]. Results are summarized in the following theorem. Here $\mathcal{D}^0_{\phi_{\max}}$ is the interior of the set $\mathcal{D}_{\phi_{\max}} := \{\Phi \in \mathbb{R}^N : \phi_1 \ge 0,\dots,\phi_N \ge 0,\ \phi \le \phi_{\max}\}$, where $0 < \phi_{\max} \le 1$ is a maximal solids concentration.

THEOREM 2.1. *If $\delta_1 > \delta_2 > \cdots > \delta_N$ and $\Phi \in \mathcal{D}^0_{\phi_{\max}}$, then the system (1.2) with $\boldsymbol{B}(\Phi) = 0$ and $\boldsymbol{f}(\Phi)$ defined by* (2.3) *is strictly hyperbolic, i.e., $\mathcal{J}_{\boldsymbol{f}}(\Phi)$ has N distinct real eigenvalues $\lambda_1,\dots,\lambda_N$ which are the roots of the so-called* secular equation

$$R(\lambda) := 1 + \sum_{j=1}^{N} \frac{\gamma_j}{v_j - \lambda}, \tag{2.9}$$

where γ_j can be computed explicitly as $\gamma_j = -v_1(0)(n_{\mathrm{RZ}} - 1)(1-\phi)^{n_{\mathrm{RZ}}-2}\phi_j\delta_j$. Moreover, the following so-called interlacing property holds:

$$v_N < \lambda_N < v_{N-1} < \lambda_{N-1} < \cdots < v_1 < \lambda_1 < M_2 := v_1 + \gamma_1 + \cdots + \gamma_N.$$

With respect to the diffusion matrix $\boldsymbol{B}(\Phi)$, in [5] it is proved that its eigenvalues are positive and pairwise distinct on $\mathcal{D}^0_{\phi_{\max}}\backslash\mathcal{D}_{\phi_{\mathrm{c}}}$ by evaluating the characteristic polynomial in a fashion similar to that used for the eigenvalues of $\mathcal{J}_{\boldsymbol{f}}(\Phi)$.

THEOREM 2.2. *Let $G(\phi) := \phi(1-\phi)^2\sigma_{\mathrm{e}}'(\phi) - \sigma_{\mathrm{e}}(\phi)$, $W(\phi) := \mu V(\phi)/(g\phi)$ and assume that $V(\phi) \ne 0$ for $\phi < \phi_{\max}$ and $V(\phi) = 0$ otherwise. Then, for all $\Phi \in \mathcal{D}^0_{\phi_{\max}}\backslash\mathcal{D}_{\phi_{\mathrm{c}}}$ the matrix $\boldsymbol{B}(\Phi)$ has N distinct positive eigenvalues $\Lambda_1,\dots,\Lambda_N$; i.e. the system* (1.2) *is strictly parabolic on $\Phi \in \mathcal{D}^0_{\phi_{\max}}\backslash\mathcal{D}_{\phi_{\mathrm{c}}}$. Moreover, we have the following interlacing properties, where for brevity we write $W = W(\phi)$ and $\sigma_{\mathrm{e}} = \sigma_{\mathrm{e}}(\phi)$:*

1. *If Φ is chosen such that $G(\phi) > 0$, then these eigenvalues satisfy*

$$0 < W\sigma_{\mathrm{e}}\delta_N < \Lambda_N < W\sigma_{\mathrm{e}}\delta_{N-1} < \cdots < W\sigma_{\mathrm{e}}\delta_1 < \Lambda_N < W\delta_1\phi(1-\phi)^2\sigma_{\mathrm{e}}'(\phi).$$

2. *At those points Φ where $G(\phi) < 0$, we have*

$$0 < W\sigma_{\mathrm{e}}\phi(1-\phi)^2\delta_N < \Lambda_N < W\sigma_{\mathrm{e}}\delta_{N-1} < \cdots < W\sigma_{\mathrm{e}}\delta_1 < \Lambda_N < W\delta_1\sigma_{\mathrm{e}}'(\phi).$$

3. *If $G(\phi) = 0$, then the eigenvalues are given by $\Lambda_i = W\sigma_{\mathrm{e}}\delta_i$ for $i = 1, \ldots, N$.*

2.3. A diffusively corrected MCLWR model. We now derive a multi-class version of the diffusively corrected kinematic traffic flow model introduced in [30] (see also [10, 31]) for $N = 1$. Assume now that ϕ_i, $i = 1, \ldots, N$, is the density, measured in vehicles per mile, of vehicles of class i having the preferential velocity $v_i^{\max}$, where

$$v_1^{\max} > v_2^{\max} > \cdots > v_N^{\max} > 0. \tag{2.10}$$

According to the MCLWR model [4, 42], the local velocity v_i of vehicles of species i is given by $v_i = v_i^{\max}V(\phi)$, where $v_i^{\max}$ is the preferential velocity of drivers of species i on a free highway, as usual, $\phi = \phi_1 + \cdots + \phi_N$, and V is a non-increasing function satisfying $V(0) = 1$, $V(\phi_{\max}) = 0$, and $V'(\phi) \le 0$ for $0 \le \phi \le \phi_{\max}$. Thus, the standard MCLWR model (without diffusive correction) is given by (1.1), where

$$f_i(\Phi) = \phi_i v_i^{\max}V(\phi), \quad i = 1, \ldots, N. \tag{2.11}$$

Let us now assume that the behavior of drivers of species i is associated with an anticipation distance L_i and a reaction time τ_i, $i = 1, \ldots, N$. Then, following the reasoning in [10], the reaction of the driver does not depend on the value of ϕ seen at the point $\phi(x,t)$, but rather on $p_i(x,t) := \phi(x + L_i - v_i^{\max}V\tau_i, t - \tau_i)$. This formulation takes into account that $v_i^{\max}V\tau_i$ is the distance travelled by a car of species i in a time interval of length τ_i. (Note that notation is ambiguous here, since we are not specific about the argument of V, cf. [10].) To obtain a usable expression for the flux f_i, we expand $V(p_i(x,t))$ around $\phi(x,t)$. Writing $\phi = \phi(x,t)$ and denoting $\tau := \max\{\tau_1, \ldots, \tau_N\}$, $L := \max\{L_1, \ldots, L_N\}$, we obtain

$$V(p_i(x,t)) = V(\phi) + V'(\phi)\big[\partial_x\phi\big(L_i - v_i^{\max}V(\phi)\tau_i\big) - \tau_i\partial_t\phi\big] + \mathcal{O}(\tau^2 + L^2). \tag{2.12}$$

On the other hand, summing the conservation laws $\partial_t\phi_i + \partial_x(v_i^{\max}\phi_i V(\phi)) = 0$ over $i = 1, \ldots, N$ and defining $\boldsymbol{v}^{\max} := (v_1^{\max}, \ldots, v_N^{\max})^{\mathrm{T}}$, we get

$$\partial_t\phi = \partial_t\phi_1 + \cdots + \partial_t\phi_N = -\partial_x\big(V(\phi)(\boldsymbol{v}^{\max})^{\mathrm{T}}\Phi\big).$$

Inserting this result into (2.12) we get

$$\begin{aligned} V(p_i(x,t)) = V(\phi) + V'(\phi)\big[\big(L_i - \tau_i v_i^{\max}V(\phi)\big)\partial_x\phi + \tau_i\partial_x\big(V(\phi)(\boldsymbol{v}^{\max})^{\mathrm{T}}\Phi\big)\big] \\ + \mathcal{O}(\tau^2 + L^2). \end{aligned}$$

Neglecting the $\mathcal{O}(\tau^2+L^2)$ term and inserting the result into the conservation equations

$$\partial_t\phi_i(x,t) + \partial_x\big(\phi_i(x,t)v_i(x,t)\big) = 0, \quad v_i(x,t) = v_i^{\max}V\big(p_i(x,t)\big), \quad i = 1, \ldots, N,$$

we obtain a system of the form (1.2), where the components of the flux vector $\boldsymbol{f}(\Phi)$ are given by (2.11) and the entries of the diffusion matrix $\boldsymbol{B}(\Phi)$ are now given by

$$\begin{aligned} \alpha_{ij}(\Phi) = -V'(\phi)\big[L_i + \tau_i\big(V'(\phi)(\boldsymbol{v}^{\max})^{\mathrm{T}}\Phi + \big(v_j^{\max} - v_i^{\max}\big)V(\phi)\big)\big]\phi_i v_i^{\max}, \\ 1 \le i, j \le N. \end{aligned} \tag{2.13}$$

For traffic flow models we will use periodic boundary conditions corresponding to a circular road of length K, namely

$$\boldsymbol{\Phi}(0,t) = \boldsymbol{\Phi}(K,t), \quad t > 0. \tag{2.14}$$

2.4. Hyperbolicity and parabolicity analysis for the diffusively corrected MCLWR model. According to [17], the MCLWR model (1.2) with $\boldsymbol{B} \equiv 0$ is strictly hyperbolic and the Jacobian $\mathcal{J}_{\boldsymbol{f}}(\Phi)$ is a rank-one perturbation of a diagonal matrix. The eigenstructure of $\mathcal{J}_{\boldsymbol{f}}(\Phi)$ can again be computed via the secular equation [2], as is explained in the following version of Theorem 2.1.

THEOREM 2.3. *Consider the first-order multiclass kinematic traffic flow model* (1.1), (2.11) *(i.e., without diffusive terms) and assume that the velocities* $v_i^{\max}$ *are ordered according to* (2.10)*). If* $\Phi \in \mathcal{D}_1^0$*, then the Jacobian* $\mathcal{J}_{\boldsymbol{f}}(\Phi)$ *has* N *distinct real eigenvalues* $\lambda_1, \dots, \lambda_N$ *which are the roots of the secular equation* (2.9) *with* $\gamma_i = v_i^{\max}\phi_i V'(\phi)$*, and the following interlacing property holds:*

$$v_N^{\max} + V'(\phi)(\boldsymbol{v}^{\max})^{\mathrm{T}}\Phi < \lambda_N < v_N^{\max} < \lambda_{N-1} < v_{N-1}^{\max} < \cdots < v_2^{\max} < \lambda_1 < v_1^{\max}.$$

We now wish to state sufficient conditions on the non-negative parameters $v_i^{\max}$, τ_i and L_i under which $\boldsymbol{B}(\Phi)$ has eigenvalues with positive real part for all $\Phi \in \mathcal{D}_{\phi_{\max}}$. The latter property will only hold under restrictions on the parameters L_i and τ_i. In fact, already in the case $N = 1$, where $B(\phi) = -V'(\phi)(L + \tau v_{\max}\phi V'(\phi))\phi v_{\max}$, and considering that $V'(\phi) \le 0$, we get that $B(\phi) \ge 0$ for all $0 \le \phi \le \phi_{\max}$ if and only if

$$\phi V'(\phi) \ge -\frac{L}{\tau v_{\max}} \quad \text{for all } 0 \le \phi \le \phi_{\max}. \tag{2.15}$$

Thus, we cannot expect $\boldsymbol{B}(\Phi)$ to have non-negative eigenvalues only without further limitations and structural conditions between the parameters $v_i^{\max}$, L_i and τ_i.

LEMMA 2.4. *The eigenvalues* $\mu_1, \dots, \mu_N$ *of* $\boldsymbol{B}(\Phi)$ *are given by* $\mu_i = -V'(\phi)\lambda_i$*,* $i = 1, \dots, N$*, where*

$$\lambda_1 = \frac{C_1}{2} - \left(\frac{C_1^2}{4} - C_2\right)^{1/2}, \quad \lambda_2 = \frac{C_1}{2} + \left(\frac{C_1^2}{4} - C_2\right)^{1/2}, \quad \lambda_3 = \cdots = \lambda_N = 0,$$

where we have

$$\begin{aligned} C_1 &= \sum_{k=1}^{N} \phi_k v_k^{\max}\big(L_k + \tau_k V'(\phi)(\boldsymbol{v}^{\max})^{\mathrm{T}}\Phi\big), \\ C_2 &= \sum_{\substack{i,j=1 \\ i<j}}^{N} \phi_i v_i^{\max}\phi_j v_j^{\max}\tau_i\tau_j \left(\frac{L_i}{\tau_i} - \frac{L_j}{\tau_j} + (v_j^{\max} - v_i^{\max})V(\phi)\right)(v_j^{\max} - v_i^{\max})V(\phi). \end{aligned} \tag{2.16}$$

Proof. We have $\boldsymbol{B}(\Phi) = -V'(\phi)\tilde{\boldsymbol{B}}(\Phi)$, where $\tilde{\boldsymbol{B}}(\Phi) = (\tilde{\alpha}_{ij}(\Phi))_{1\le i,j\le N}$ is defined in an obvious manner via (2.13). (Clearly, since $V'(\phi) \le 0$, $\boldsymbol{B}(\Phi)$ has non-negative eigenvalues on $\mathcal{D}_{\phi_{\max}}$ if $\tilde{\boldsymbol{B}}(\Phi)$ has.) Since $\tilde{\boldsymbol{B}}(\Phi)$ is a rank-2 matrix of size $N \times N$, we know that $\det(\lambda \boldsymbol{I} - \tilde{\boldsymbol{B}}(\Phi)) = \lambda^{N-2}(\lambda^2 - C_1\lambda + C_2)$, where $C_k = C_k(\Phi)$ is the sum of the k-rowed principal minors of $\tilde{\boldsymbol{B}}(\Phi)$, that is,

$$C_1 = \operatorname{tr}\tilde{\boldsymbol{B}}(\Phi), \quad C_2 = \sum_{\substack{i,j=1 \\ i<j}}^{N} \big(\tilde{\alpha}_{ii}\tilde{\alpha}_{jj} - \tilde{\alpha}_{ji}\tilde{\alpha}_{ij}\big). \tag{2.17}$$

From (2.13) we get that $\tilde{\alpha}_{ij} = (L_i + \tau_i V'(\phi)(\boldsymbol{v}^{\max})^{\mathrm{T}}\Phi + \tau_i(v_j^{\max} - v_i^{\max})V(\Phi))\phi_i v_i^{\max}$ for $i, j = 1, \ldots, N$. Evaluating (2.17) then yields (2.16). □

We recall that the system (1.2) is called *parabolic* at a state Φ_0 if the eigenvalues of $\boldsymbol{B}(\Phi_0)$ have non-negative real parts. This is precisely the case if $C_1(\Phi_0) \geq 0$ and $C_2(\Phi_0) \geq 0$. Thus, we can expect the system to be well-posed only if

$$C_1(\Phi) > 0, \quad C_2(\Phi) > 0 \quad \text{on } \mathcal{D}^0_{\phi_{\max}}. \tag{2.18}$$

In view of $V'(\phi)(\boldsymbol{v}^{\max})^{\mathrm{T}}\Phi \leq 0$, a sufficient condition for $C_1(\Phi) \geq 0$ to hold is that

$$L_k(\phi) + \tau_k v_1^{\max}\phi V'(\phi) \leq 0 \quad \text{for } 0 \leq \phi \leq \phi_{\max},\ k = 1, \ldots, N. \tag{2.19}$$

Note that this condition is the multi-class ($N \geq 1$) extension of (2.15). Furthermore, note that we can write (2.19) as

$$\tau_k \leq \min_{0 \leq \phi \leq \phi_{\max}} -\frac{L_k(\phi)}{\phi V'(\phi) v_1^{\max}}. \tag{2.20}$$

If (2.20) is violated, that is, when the reaction time of a driver is not sufficiently small, then the model is likely to exhibit anti-diffusive phenomena such as formation of clusters, steep density gradients, stop-and-go waves, and other instability phenomena. A similar conclusion (though based on a slightly different model) has been drawn, for example, in [33]. For the diffusively corrected MCLWR model we will expand on this observation, and more closely analyze instability phenomena, in a separate paper.

In the case $N = 1$, Nelson [30] (cf. [10, 31]) suggests to employ

$$L = L(\phi) = \max\left\{\frac{(v_{\max}V(\phi))^2}{2a}, L_{\min}\right\}, \tag{2.21}$$

where the first argument is the distance required to decelerate to full stop from speed $v_{\max}V(\phi)$ at deceleration a, and the second is a minimal anticipation distance $L_{\min} > 0$ regardless of how small the velocity is. In the multi-class case we could define L_i, for instance, by (2.21) with $v_{\max}$ replaced by $v_i^{\max}$. However, in our numerical experiments, we select L_i and τ_i constant to ensure that (2.18) is always satisfied.

3. Numerical schemes.

3.1. Spatial discretization. For grid points $x_j := (j - \frac{1}{2})\Delta x$ for $j = 1, \ldots, M$, where $\Delta x := K/M$, and $t_n := n\Delta t$ for $n \in \mathbb{N}_0$, and using the notation $\Delta^- \boldsymbol{g}_k = \boldsymbol{g}_k - \boldsymbol{g}_{k-1}$ we discretize (1.2) in space as follows:

$$\frac{\mathrm{d}\Phi_j(t)}{\mathrm{d}t} = \mathcal{L}_j(\boldsymbol{\Phi}) := -\frac{1}{\Delta x}\Delta^- \boldsymbol{f}_{j+1/2} + \frac{1}{\Delta x}\Delta^- \boldsymbol{g}_{j+1/2}, \quad j = 1, \ldots, M, \tag{3.1}$$

where $\Phi_j(t) \approx \Phi(x_j, t)$ and the convective numerical flux $\boldsymbol{f}_{j+1/2} := \boldsymbol{f}(\Phi_{j-2}, \ldots, \Phi_{j+3})$ is calculated by using the characteristic-wise fifth-order WENO-approximation [9] and the flux corresponding to the parabolic term is given by

$$\boldsymbol{B}(\Phi)\partial_x\Phi|_{x=x_{j+1/2}} \approx \boldsymbol{g}_{j+1/2} := \frac{1}{2\Delta x}\big(\boldsymbol{B}(\Phi_{j+1}) + \boldsymbol{B}(\Phi_j)\big)\Delta^-\Phi_{j+1},$$

which gives a second-order approximation for the diffusive term. Higher order approximations of these terms could be used to match the order of approximation of the convective term, but we will not pursue this issue in this paper.

The operator $\boldsymbol{\mathcal{L}} := (\mathcal{L}_1, \dots, \mathcal{L}_M)^{\mathrm{T}}$ appearing in the semi-discrete scheme (3.1) for (1.2) is now given by

$$\mathcal{L}_j(\boldsymbol{\Phi}) = -\frac{1}{\Delta x}\Delta^- \boldsymbol{f}_{j+1/2} + \frac{1}{2\Delta x^2}\Delta^-\Big(\big(\boldsymbol{B}(\Phi_{j+1}) + \boldsymbol{B}(\Phi_j)\big)\Delta^-\Phi_{j+1}\Big)$$

for $j = 2, \dots, M-1$, along with appropriate modifications of this formula for $j = 1$ and $j = M$ to account for boundary conditions. This can be further written as follows:

$$\boldsymbol{\mathcal{L}}(\boldsymbol{\Phi}) = -\frac{1}{\Delta x}(\Delta^- \boldsymbol{f})(\boldsymbol{\Phi}) + \frac{1}{\Delta x^2}\boldsymbol{\mathcal{B}}(\boldsymbol{\Phi})\boldsymbol{\Phi}, \tag{3.2}$$

where $\boldsymbol{\mathcal{B}}(\boldsymbol{v}) = \{\boldsymbol{\mathcal{B}}_{ij}(\boldsymbol{v})\}_{i,j=1,\dots,M} \in \mathbb{R}^{(NM)\times(NM)}$ is a block tridiagonal matrix formed by blocks $\boldsymbol{\mathcal{B}}_{ij} \in \mathbb{R}^{N\times N}$ generally given by

$$\begin{aligned}
\boldsymbol{\mathcal{B}}_{ii}(\boldsymbol{v}) &= \frac{1}{2\Delta x^2}\big(\boldsymbol{B}(\boldsymbol{v}_{i+1}) + 2\boldsymbol{B}(\boldsymbol{v}_i) + \boldsymbol{B}(\boldsymbol{v}_{i-1})\big), \quad i = 1, \dots, M,\\
\boldsymbol{\mathcal{B}}_{i,i-1}(\boldsymbol{v}) &= \boldsymbol{\mathcal{B}}_{i-1,i}(\boldsymbol{v}) = -\frac{1}{2\Delta x^2}\big(\boldsymbol{B}(\boldsymbol{v}_{i-1}) + \boldsymbol{B}(\boldsymbol{v}_i)\big), \quad i = 2, \dots, M.
\end{aligned} \tag{3.3}$$

3.2. Boundary conditions. For the polydisperse sedimentation model we discretize the zero-flux boundary conditions (2.2) by setting $\boldsymbol{f}_{1/2} - \boldsymbol{g}_{1/2} = \boldsymbol{0}$ and $\boldsymbol{f}_{M+1/2} - \boldsymbol{g}_{M+1/2} = \boldsymbol{0}$. This affects $\mathcal{L}_1$ and $\mathcal{L}_M$, which now read as

$$\begin{aligned}
\mathcal{L}_1(\boldsymbol{\Phi}) &= -\frac{1}{\Delta x}\boldsymbol{f}_{3/2} + \frac{1}{2\Delta x^2}\big(\boldsymbol{B}(\Phi_2) + \boldsymbol{B}(\Phi_1)\big)\Delta^-\Phi_2,\\
\mathcal{L}_M(\boldsymbol{\Phi}) &= \frac{1}{\Delta x}\boldsymbol{f}_{M-1/2} - \frac{1}{2\Delta x^2}\big(\boldsymbol{B}(\Phi_{M-1}) + \boldsymbol{B}(\Phi_M)\big)\Delta^-\Phi_M.
\end{aligned}$$

This can be written as (3.2) with

$$\boldsymbol{\mathcal{B}}_{11}(\boldsymbol{v}) = \frac{1}{2\Delta x^2}\big(\boldsymbol{B}(\boldsymbol{v}_2) + \boldsymbol{B}(\boldsymbol{v}_1)\big), \quad \boldsymbol{\mathcal{B}}_{MM}(\boldsymbol{v}) = \frac{1}{2\Delta x^2}\big(\boldsymbol{B}(\boldsymbol{v}_{M-1}) + \boldsymbol{B}(\boldsymbol{v}_M)\big).$$

When we discretize the periodic boundary conditions (2.14), for the discretization of the flux at $x = 0$ we formally need values Φ_{-j} for $j = 0, 1, 2$. By periodicity the value Φ_{-j} should agree with the value Φ_{M-j}. Similarly, at $x = K$ the value Φ_{M+j}, $j = 1, 2, 3$, should agree with Φ_j. Therefore, we have the following:

$$\begin{aligned}
\mathcal{L}_1(\boldsymbol{\Phi}) = &-\frac{1}{\Delta x}\Delta^- \boldsymbol{f}_{3/2} + \frac{1}{2\Delta x^2}\Big(\big(\boldsymbol{B}(\Phi_2) + \boldsymbol{B}(\Phi_1)\big)\Delta^-\Phi_2\\
&\qquad - \big(\boldsymbol{B}(\Phi_1) + \boldsymbol{B}(\Phi_M)\big)(\Phi_1 - \Phi_M)\Big),\\
\mathcal{L}_M(\boldsymbol{\Phi}) = &-\frac{1}{\Delta x}\Delta^- \boldsymbol{f}_{M+1/2} + \frac{1}{2\Delta x^2}\Big(\big(\boldsymbol{B}(\Phi_M) + \boldsymbol{B}(\Phi_1)\big)(\Phi_1 - \Phi_M)\\
&\qquad - \big(\boldsymbol{B}(\Phi_{M-1}) + \boldsymbol{B}(\Phi_M)\big)\Delta^-\Phi_M\Big).
\end{aligned}$$

The blocks in the first and last rows of blocks of matrix $\boldsymbol{\mathcal{B}}$ in (3.3) that should be modified with respect to the general definition are:

$$\begin{aligned}
\boldsymbol{\mathcal{B}}_{11}(\boldsymbol{v}) &= \frac{1}{2\Delta x^2}\big(\boldsymbol{B}(\boldsymbol{v}_2) + 2\boldsymbol{B}(\boldsymbol{v}_1) + \boldsymbol{B}(\boldsymbol{v}_M)\big),\\
\boldsymbol{\mathcal{B}}_{MM}(\boldsymbol{v}) &= \frac{1}{2\Delta x^2}\big(\boldsymbol{B}(\boldsymbol{v}_1) + 2\boldsymbol{B}(\boldsymbol{v}_M) + \boldsymbol{B}(\boldsymbol{v}_{M-1})\big),\\
\boldsymbol{\mathcal{B}}_{1,M}(\boldsymbol{v}) &= -\frac{1}{2\Delta x^2}\big(\boldsymbol{B}(\boldsymbol{v}_1) + \boldsymbol{B}(\boldsymbol{v}_M)\big), \quad \boldsymbol{\mathcal{B}}_{M,1}(\boldsymbol{v}) = -\frac{1}{2\Delta x^2}\big(\boldsymbol{B}(\boldsymbol{v}_1) + \boldsymbol{B}(\boldsymbol{v}_M)\big).
\end{aligned}$$

Therefore, the block structure of $\boldsymbol{\mathcal{B}}$ turns out to be *circulant* tridiagonal.

3.3. Explicit schemes. Given an approximation $\boldsymbol{\Phi}^n = (\Phi_1^n, \dots, \Phi_M^n)^{\mathrm{T}}$ for $t = t_n$, we can compute an approximation $\boldsymbol{\Phi}^{n+1} = (\Phi_1^{n+1}, \dots, \Phi_M^{n+1})^{\mathrm{T}}$ for $t = t_{n+1}$ from (3.1) by using an ODE solver, such as Euler's method or third-order TVD Runge-Kutta method (see [20, 21, 40]). For instance, Euler's method can be written as

$$\boldsymbol{\Phi}^{n+1} = \boldsymbol{\Phi}^n - \frac{\Delta t}{\Delta x}(\Delta \boldsymbol{f})(\boldsymbol{\Phi}^n) + \frac{\Delta t}{\Delta x^2}\boldsymbol{\mathcal{B}}(\boldsymbol{\Phi}^n)\boldsymbol{\Phi}^n. \tag{3.4}$$

Other explicit schemes, such as the KT scheme [24] that we use in our numerical experiments, have a similar formulation.

A von Neumann analysis of the stability of these explicit schemes applied to suitable linearizations about constant states would suggest that

$$\frac{\Delta t}{\Delta x}\max_{\Phi}\rho(\mathcal{J}_{\boldsymbol{f}}(\Phi)) + \frac{\Delta t}{2\Delta x^2}\max_{\Phi}\rho(\boldsymbol{B}(\Phi)) \le C \le 1 \tag{3.5}$$

is an appropriate CFL stability condition, where $\rho(\cdot)$ is the spectral radius. The constant C depends on the method and should be empirically adjusted for nonlinear problems, since (3.5) is deduced for linearized problems and schemes.

3.4. Implicit-explicit schemes. The CFL stability condition (3.5) restricts the time step size dramatically when $\boldsymbol{B}(\Phi) \neq 0$. This restriction could be overcome by implicit schemes, but the implicit treatment of the convective term is complicated due to the highly nonlinear scheme that is used for its discretization. Therefore, implicit-explicit (IMEX) schemes, which treat the diffusive term implicitly and the convective term explicitly, could be an attractive alternative in this situation. The simplest IMEX scheme for the approximation of (3.1) is the following version of (3.4):

$$\boldsymbol{\Phi}^{n+1} = \boldsymbol{\Phi}^n - \frac{\Delta t}{\Delta x}(\Delta \boldsymbol{f})(\boldsymbol{\Phi}^n) + \frac{\Delta t}{\Delta x^2}\boldsymbol{\mathcal{B}}(\boldsymbol{\Phi}^{n+1})\boldsymbol{\Phi}^{n+1}. \tag{3.6}$$

The CFL condition for IMEX schemes is

$$\frac{\Delta t}{\Delta x}\max_{\Phi}\rho(\mathcal{J}_{\boldsymbol{f}}(\Phi)) \le C_1 \le 1,$$

which is much less restrictive than (3.5). Here, as mentioned above, the constant C_1 depends on the method used for the spatial and temporal discretizations.

For the case of zero-flux boundary conditions, the boundary condition at $x = 0$ for the scheme (3.6) should be $\boldsymbol{f}_{1/2}^k - \boldsymbol{g}_{1/2}^k = \boldsymbol{0}$ for $k = n$ or $k = n+1$. The use of different treatments for the convective and diffusive parts does not allow us to impose this condition in a natural manner as for explicit schemes. However, we impose this condition to avoid adding ghost cells and changing the structure of the matrices, but this treatment does generate a loss of precision at the boundary. In this manner we use for $j = 1$ the equation

$$\Phi_1^{n+1} = \Phi_1^n - \frac{\Delta t}{\Delta x}\boldsymbol{f}_{3/2}^n + \frac{\Delta t}{\Delta x^2}\big(\boldsymbol{B}(\Phi_2^{n+1}) + \boldsymbol{B}(\Phi_1^{n+1})\big)\Delta^-\Phi_2^{n+1}.$$

The boundary condition at $x = K$ is treated in a similar way. For periodic boundary conditions (cf. Section 3.2), the equations for $j = 1$ and $j = M$ in (3.6) are

$$\Phi_1^{n+1} = \Phi_1^n - \frac{\Delta t}{\Delta x}\Delta^-\boldsymbol{f}_{3/2}^n + \frac{\Delta t}{2\Delta x^2}\Big(\big(\boldsymbol{B}(\Phi_2^{n+1}) + \boldsymbol{B}(\Phi_1^{n+1})\big)\Delta^-\Phi_2^{n+1}$$

$$- \big(\boldsymbol{B}(\Phi_1^{n+1}) + \boldsymbol{B}(\Phi_M^{n+1})\big)\,\big(\Phi_1^{n+1} - \Phi_M^{n+1}\big)\Big),$$

$$\Phi_M^{n+1} = \Phi_M^n - \frac{\Delta t}{\Delta x}\Delta^- \boldsymbol{f}_{M+1/2}^n + \frac{\Delta t}{2\Delta x^2}\Big(\big(\boldsymbol{B}(\Phi_M^{n+1}) + \boldsymbol{B}(\Phi_1^{n+1})\big)\,\big(\Phi_1^{n+1} - \Phi_M^{n+1}\big)\big)$$
$$- \big(\boldsymbol{B}(\Phi_{M-1}^{n+1}) + \boldsymbol{B}(\Phi_M^{n+1})\big)\Delta^-\Phi_M^{n+1}\Big).$$

3.5. IMEX Runge-Kutta schemes. To introduce IMEX methods for the initial-boundary value problems of (1.2) at hand, we basically follow the notation in [3] and rewrite the semi-discrete formulation (3.1) in the form (1.3), where

$$C(\boldsymbol{\Phi}) := -\frac{1}{\Delta x}(\Delta \boldsymbol{f})(\boldsymbol{\Phi}), \quad D(\boldsymbol{\Phi}) := \frac{1}{\Delta x^2}\boldsymbol{\mathcal{B}}(\boldsymbol{\Phi})\boldsymbol{\Phi}.$$

For the diffusive part we utilize an implicit s-stage diagonally implicit (DIRK) scheme with coefficients $\boldsymbol{A} \in \mathbb{R}^{s\times s}$, $\boldsymbol{c}, \boldsymbol{b} \in \mathbb{R}^s$, in the common Butcher notation, where $\boldsymbol{A} = (a_{ij})$ with $a_{ij} = 0$ for $j > i$. For the convective part we employ an $s+1$-stage explicit scheme with coefficients $\hat{\boldsymbol{A}} \in \mathbb{R}^{(s+1)\times(s+1)}$, $\hat{\boldsymbol{b}}$, $\hat{\boldsymbol{c}} \in \mathbb{R}^{s+1}$ with $c_1 = 0$ and $\hat{\boldsymbol{A}} = (\hat{a}_{ij})$ with $\hat{a}_{ij} = 0$ for $j \geq i$. We will denote the corresponding Butcher arrays by

$$\boldsymbol{D} := \begin{array}{c|c} \boldsymbol{c} & \boldsymbol{A} \\ \hline & \boldsymbol{b}^{\mathrm{T}} \end{array}, \qquad \hat{\boldsymbol{D}} := \begin{array}{c|c} \hat{\boldsymbol{c}} & \hat{\boldsymbol{A}} \\ \hline & \hat{\boldsymbol{b}}^{\mathrm{T}} \end{array}.$$

The computations of an IMEX-RK scheme necessary to advance an approximate solution $\boldsymbol{\Phi}^n$ from time t^n to $t^{n+1} = t^n + \Delta t$ are given in the following algorithm.

ALGORITHM 3.1 (Implicit-explicit Runge-Kutta (IMEX-RK) scheme).

Input: approximate solution vector $\boldsymbol{\Phi}^n$ for $t = t_n$

$\hat{K}_1 \leftarrow C(\boldsymbol{\Phi}^n)$

do $i = 1, \ldots, s$

solve for $\boldsymbol{\Phi}^{(i)}$ the nonlinear equation

$$\boldsymbol{\Phi}^{(i)} = \boldsymbol{\Phi}^n + \Delta t\left(\sum_{j=1}^{i-1} a_{ij}K_j + a_{ii}D\big(\boldsymbol{\Phi}^{(i)}\big) + \sum_{j=1}^{i}\hat{a}_{i+1,j}\hat{K}_j\right)$$

$K_i \leftarrow D(\boldsymbol{\Phi}^{(i)})$

$\hat{K}_{i+1} \leftarrow C(\boldsymbol{\Phi}^{(i)})$

enddo

$$\boldsymbol{\Phi}^{n+1} \leftarrow \boldsymbol{\Phi}^n + \Delta t\sum_{j=1}^{s} b_jK_j + \Delta t\sum_{j=1}^{s+1}\hat{b}_j\hat{K}_j$$

Output: approximate solution vector $\boldsymbol{\Phi}^{n+1}$ for $t = t_{n+1} = t_n + \Delta t$.

Notice that the $(s+1)$-th stage of the explicit Runge-Kutta scheme need not be performed to compute $\hat{K}_{s+1}$ if $\hat{b}_{s+1} = 0$; in this case, we will define the *effective* number of stages σ to be s, otherwise $\sigma = s+1$.

Algorithm 3.1 requires solving for the vector $\boldsymbol{u} = \boldsymbol{\Phi}^{(i)} \in \mathbb{R}^{MN}$ a nonlinear system of NM scalar equations of the form

$$\boldsymbol{F}(\boldsymbol{u}) := \boldsymbol{u} - a_{ii}\Delta t\boldsymbol{\mathcal{B}}(\boldsymbol{u})\boldsymbol{u} - \boldsymbol{r} = \boldsymbol{0}, \tag{3.7}$$

where the vector $\boldsymbol{r} \in \mathbb{R}^{MN}$ is given by

$$\boldsymbol{r} = \boldsymbol{\Phi}^n + \Delta t\sum_{j=1}^{i-1} a_{ij}\boldsymbol{\mathcal{B}}\big(\boldsymbol{\Phi}^{(j)}\big)\boldsymbol{\Phi}^{(j)} + \Delta t\sum_{j=1}^{i}\hat{a}_{i+1,j}(\Delta \boldsymbol{f})\big(\boldsymbol{\Phi}^{(j)}\big). \tag{3.8}$$

The solution of systems (3.7), (3.8) will be discussed in Section 4.

We identify a particular IMEX-RK scheme with the notation $Name(s, \sigma, p)$, where this triplet characterizes the number s of stages of the implicit scheme, the number σ of effective stages of the explicit scheme ($\sigma = s$ or $\sigma = s + 1$) and the order p of the method. We consider the following three schemes (see [3] for more details): the scheme IMEX-RK(1,1,1) defined by the pair of Butcher arrays

$$\boldsymbol{D} = \begin{array}{c|cc} 0 & 0 & 0 \\ 1 & 0 & 1 \\ \hline & 0 & 1 \end{array}, \qquad \hat{\boldsymbol{D}} = \begin{array}{c|cc} 0 & 0 & 0 \\ 1 & 1 & 0 \\ \hline & 1 & 0 \end{array}, \tag{3.9}$$

the scheme IMEX-RK(2,2,2) defined by

$$\boldsymbol{D} = \begin{array}{c|cc} \gamma & \gamma & 0 \\ 1 & 1-\gamma & \gamma \\ \hline & 1-\gamma & \gamma \end{array}, \qquad \hat{\boldsymbol{D}} = \begin{array}{c|ccc} 0 & 0 & 0 & 0 \\ \gamma & \gamma & 0 & 0 \\ 1 & \delta & 1-\delta & 0 \\ \hline & \delta & 1-\delta & 0 \end{array}, \tag{3.10}$$

$$\text{where} \quad \gamma = 1 - \frac{1}{\sqrt{2}}, \quad \delta = 1 - \frac{1}{2\gamma},$$

and the scheme IMEX-RK(3,4,3) defined by

$$\boldsymbol{D} = \begin{array}{c|ccc} \gamma & \gamma & 0 & 0 \\ \frac{1+\gamma}{2} & \frac{1-\gamma}{2} & \gamma & 0 \\ 1 & b_1 & b_2 & \gamma \\ \hline & b_1 & b_2 & \gamma \end{array}, \quad \hat{\boldsymbol{D}} = \begin{array}{c|cccc} 0 & 0 & 0 & 0 & 0 \\ \gamma & \gamma & 0 & 0 & 0 \\ \frac{1+\gamma}{2} & \hat{a}_{31} & \hat{a}_{32} & 0 & 0 \\ 1 & \hat{a}_{41} & \hat{a}_{42} & \hat{a}_{43} & 0 \\ \hline & 0 & b_1 & b_2 & \gamma \end{array}, \tag{3.11}$$

where γ is the middle root of $6x^3 - 18x^2 + 9x - 1 = 0$, and

$$\begin{aligned} b_1 &= -\frac{3}{2}\gamma^2 + 4\gamma - \frac{1}{4}, \quad b_2 = \frac{3}{2}\gamma^2 - 5\gamma + \frac{5}{4}, \\ \hat{a}_{31} &= \left(1 - \frac{9}{2}\gamma + \frac{3}{2}\gamma^2\right)\hat{a}_{42} + \left(\frac{11}{4} - \frac{21}{2}\gamma + \frac{15}{4}\gamma^2\right)\hat{a}_{43} - \frac{7}{2} + 13\gamma - \frac{9}{2}\gamma^2, \\ \hat{a}_{32} &= \left(-1 + \frac{9}{2}\gamma - \frac{3}{2}\gamma^2\right)\hat{a}_{42} + \left(-\frac{11}{4} + \frac{21}{2}\gamma - \frac{15}{4}\gamma^2\right)\hat{a}_{43} + 4 - \frac{25}{2}\gamma + \frac{9}{2}\gamma^2, \\ \hat{a}_{41} &= 1 - \hat{a}_{42} - \hat{a}_{43}. \end{aligned} \tag{3.12}$$

4. Nonlinear solvers. The previous section shows that IMEX-RK schemes are applicable to the convection-diffusion equation at hand (1.2) as long as one can efficiently find the solution of the nonlinear system (3.7), whose existence and uniqueness is guaranteed for small enough Δt. We now introduce two alternative methods that can be employed for this purpose.

4.1. Fixed-point (FP) iteration. Due to the structure of the nonlinearity in (3.7), its solution could be obtained by a lagged diffusivity FP iteration that entails solving a convection-diffusion equation with a linear diffusion term at each iteration. For this purpose, and with reference to (3.7), we define the function $\boldsymbol{G}(\boldsymbol{u}, \boldsymbol{v}) := \boldsymbol{u} - a_{ii}\Delta t\boldsymbol{\mathcal{B}}(\boldsymbol{v})\boldsymbol{u} - \boldsymbol{r}$ for $\boldsymbol{u}, \boldsymbol{v} \in \mathbb{R}^{NM}$, which satisfies $\boldsymbol{G}(\boldsymbol{u}, \boldsymbol{u}) = \boldsymbol{F}(\boldsymbol{u})$. The algorithm starts with $\boldsymbol{u}^{(0)} = \boldsymbol{\Phi}^n$ and one solves for $\boldsymbol{u} = \boldsymbol{u}^{(\nu+1)}$ the linear system

$$\boldsymbol{G}(\boldsymbol{u}, \boldsymbol{u}^{(\nu)}) = \boldsymbol{0}, \quad \nu = 0, 1, 2, \ldots, \tag{4.1}$$

where one expects that $\boldsymbol{u}^{(\nu)}$ converges to $\boldsymbol{\Phi}^{n+1}$. This widely used linearization strategy works in some situations, but, as the following example illustrates, it may not be convergent when the diffusion coefficient is not sufficiently smooth, as is the case of equations (2.6)-(2.8) for polydisperse sedimentation and (2.13) for traffic flow models, due to the non-differentiability of the diffusion coefficients.

EXAMPLE 4.1. Consider system (3.7) for a scalar unknown ($N = 1$):

$$\frac{u_j^{n+1} - u_j^n}{\Delta t} + \frac{\hat{f}_{j+1/2} - \hat{f}_{j-1/2}}{\Delta x} = \frac{1}{\Delta x^2}\left(\frac{a_j + a_{j+1}}{2}\Delta^- u_{j+1}^{n+1} - \frac{a_{j-1} + a_j}{2}\Delta^- u_j^{n+1}\right),$$

for $j = 1, \ldots, M$, with $a_j = a(u_j^{n+1})$. For $M = 1$, $\Delta x = 1$ and Dirichlet boundary conditions $u_0 = u_2 = 0$ we obtain

$$\frac{u_1^{n+1} - u_1^n}{\Delta t} + \hat{f}_{3/2} - \hat{f}_{1/2} = \frac{a_1}{2}(-u_1^{n+1}) - \frac{a_1}{2}u_1^{n+1},$$

which can be arranged to give $u_1^{n+1}(1 + \Delta t a(u_1^{n+1})) = u_1^n - \Delta t(\hat{f}_{3/2} - \hat{f}_{1/2})$, which means that we wish to solve the equation $v(1 + \Delta t a(v)) = b := u_1^n - \Delta t(\hat{f}_{3/2} - \hat{f}_{1/2})$ for $v = u_1^{n+1}$. In this case the proposed fixed point method consists in the iteration $v^{(\nu+1)}(1 + \Delta t a(v^{(\nu)})) = b$, which gives the fixed-point iteration

$$v^{(\nu+1)} = \frac{b}{1 + \Delta t a(v^{(\nu)})} =: \varphi(v^{(\nu)}),$$

which converges for all starting values $v^{(0)}$ if $|\varphi'| < 1$. Since

$$\varphi'(v) = \frac{b\Delta t a'(v)}{(1 + \Delta t a(v))^2},$$

we see that $|\varphi'(v)| < 1$ holds if and only if $|b|\Delta t|a'(v)| < (1 + \Delta t a(v))^2$, which implies that if $|a'(v)|$ is sufficiently large, the iteration may not converge.

We therefore require an alternative nonlinear solver, such as the NR method, to handle the nonlinear systems (3.7) that arise in the present formulation.

4.2. Newton-Raphson (NR) method. To approximately solve the nonlinear system (3.7) by the NR iterative method it is necessary that the coefficients of the matrix function $\boldsymbol{B}$, and therefore those of $\boldsymbol{\mathcal{B}}$, be at least twice continuously differentiable. However, the models of interest here, namely the diffusively corrected polydisperse sedimentation and MCLWR models, do not naturally satisfy this assumption. We therefore replace $\boldsymbol{B}$ by a smooth approximation $\boldsymbol{B}_\varepsilon$, and denote the corresponding version of $\boldsymbol{\mathcal{B}}$ by $\boldsymbol{\mathcal{B}}_\varepsilon$, where it is understood that $\boldsymbol{B}_\varepsilon \to \boldsymbol{B}$ and $\boldsymbol{\mathcal{B}}_\varepsilon \to \boldsymbol{\mathcal{B}}$ as $\varepsilon \to 0$. The precise algebraic form of this approximation is defined separately for each specific application in section 5. Note that the purpose of this approximation is to create smoothness, but not to convert the problem into a uniformly parabolic one.

We denote by $\boldsymbol{F}_\varepsilon(\boldsymbol{u})$ the function (3.7), where $\boldsymbol{\mathcal{B}}(\boldsymbol{u})$ has been replaced by $\boldsymbol{\mathcal{B}}_\varepsilon(\boldsymbol{u})$. The function $\boldsymbol{F}_\varepsilon$ is highly nonlinear for small ε, in the sense that the second derivative of $\boldsymbol{F}_\varepsilon$ is much larger than its first derivative. Therefore, by Kantorovich's theorem (see [13]), the region of guaranteed convergence gets smaller when $\varepsilon \to 0$. On the other hand, the linearity of $\boldsymbol{F}_\varepsilon$ behaves in the opposite way when increasing ε (in fact, for the regularization that we use in section 5, $\boldsymbol{F}_\varepsilon(\boldsymbol{u}) \to \boldsymbol{u} - \boldsymbol{r}$, when $\varepsilon \to \infty$), so the region of guaranteed convergence of the NR method increases. With these observations, we use a similar strategy as the one used in [12] to efficiently solve $\boldsymbol{F}_\varepsilon(u) = 0$ for a prescribed $\varepsilon = \varepsilon_{\min}$ as follows:

If $\boldsymbol{u}_\varepsilon$ is a solution of $\boldsymbol{F}_\varepsilon(\boldsymbol{u}_\varepsilon)=\boldsymbol{0}$, then we use $\boldsymbol{u}_\varepsilon$ as an initial datum for approximating the solution of $\boldsymbol{F}_{\varepsilon'}(\boldsymbol{u})=\boldsymbol{0}$ for $\varepsilon'<\varepsilon$ by the NR method with a line search strategy (see [13]). We start this process with a sufficiently large value ε_0 and we repeat this process until we obtain a solution $\boldsymbol{F}_{\varepsilon_{\min}}(\boldsymbol{u})=\boldsymbol{0}$. Based on the previous discussion on the linearity of $\boldsymbol{F}_\varepsilon$, we select ε_0 as the smallest power of 10 for which the NR method succeeds (i.e., converges within a given tolerance and a generously large maximum number of iterations) solving $\boldsymbol{F}_{\varepsilon_0}(\boldsymbol{u})=0$ when given $\boldsymbol{u}=\Phi^n$ as the initial guess.

The decrease of ε can be automated by using that $\lim_{\varepsilon\to\varepsilon'}\boldsymbol{u}_\varepsilon=\boldsymbol{u}_{\varepsilon'}$ enables us to choose $\varepsilon'=\kappa\varepsilon$ for some $\kappa\in(0,1)$ and use $\boldsymbol{u}_\varepsilon$ as the initial iteration to solve $\boldsymbol{F}_{\varepsilon'}(\boldsymbol{u})$, hoping that this initial guess is close enough to the solution for the NR method to converge within a given tolerance and a given maximum number of iterations. If the NR method does not succeed, then we take κ closer to 1 and try again; on the other hand, if the NR method takes a small number of iterations to converge (less than 3, say), then we diminish the factor κ.

It is easy to see that the direction obtained from the NR method for the solution of $\boldsymbol{F}_\varepsilon(\boldsymbol{u})=\boldsymbol{0}$, namely the vector $(-\mathcal{J}_{\boldsymbol{F}_\varepsilon}(\boldsymbol{u}))^{-1}\boldsymbol{F}_\varepsilon(\boldsymbol{u})$, is a direction of descent for $m(\boldsymbol{u})=\|\boldsymbol{F}_\varepsilon(\boldsymbol{u})\|_2^2$. Therefore we can use the following algorithm to ensure the convergence of the NR method.

ALGORITHM 4.1 (Newton-Raphson (NR) method with line search strategy).

Input: approximate solution vector $\boldsymbol{\Phi}^n$ *at* $t=t_n$ *as a starting value*
$\boldsymbol{u}^{(0)}\leftarrow\boldsymbol{\Phi}^n$, $\varepsilon\leftarrow\varepsilon_0$, $m(\boldsymbol{u})\leftarrow\|\boldsymbol{F}_\varepsilon(\boldsymbol{u}^{(0)})\|_2^2$, $\nu\leftarrow 0$
while $\varepsilon\geq\varepsilon_{\min}$ **do**
  while $\nu\leq N_{\text{iter}}$ **and** $m(\boldsymbol{u}^{(\nu)})<\text{tol}$ **do**
    solve for $\boldsymbol{p}_\nu$ *the linear system* $\mathcal{J}_{\boldsymbol{F}_\varepsilon}(\boldsymbol{u}^{(\nu)})\boldsymbol{p}_\nu=-\boldsymbol{F}_\varepsilon(\boldsymbol{u}^{(\nu)})$
    $\alpha_0\leftarrow 1$
    $k\leftarrow 0$
    while $\alpha_k\geq\alpha_{\min}$ **do**
      $\boldsymbol{u}\leftarrow\boldsymbol{u}^{(\nu)}+\alpha_k\boldsymbol{p}_\nu$, $m(\boldsymbol{u})\leftarrow\|\boldsymbol{F}_\varepsilon(\boldsymbol{u})\|_2^2$
      if $m(\boldsymbol{u})<m(\boldsymbol{u}^{(\nu)})$ **then**
        $\boldsymbol{u}^{(\nu+1)}\leftarrow\boldsymbol{u}$
      else
        $\alpha_{k+1}\leftarrow 0.8\alpha_k$
      endif
      $k\leftarrow k+1$
    endwhile
    $\nu\leftarrow\nu+1$
  endwhile
  Decrease ε
endwhile
Output: approximate solution $\boldsymbol{u}$ *of the nonlinear system* $\boldsymbol{F}_\varepsilon(\boldsymbol{u})=\boldsymbol{0}$.

Since $\mathcal{J}_{\boldsymbol{F}_\varepsilon}(\boldsymbol{u})$ is a block tridiagonal (and block circulant for periodic boundary conditions) matrix, we can use an efficient block tridiagonal solver for the linear systems $\mathcal{J}_{\boldsymbol{F}_\varepsilon}(\boldsymbol{u})\boldsymbol{z}=-\boldsymbol{F}_\varepsilon(\boldsymbol{u})$. We cannot ensure the invertibility of these matrices (only for sufficiently small Δt) but have not experienced any invertibility failures in our tests.

5. Numerical results. For comparison purposes, we compute reference solutions for numerical tests by the KT scheme [24], which is employed in [5] for the numerical solution of (1.2) for the diffusively corrected polydisperse sedimentation

model (sedimentation with compression). The reference solution is based on a fine discretization with $M_{\rm ref} = 12800$ cells and Δt is selected at each time step following the formula

$$\Delta t = C_{\rm cfl1}\Big(\frac{\max_\Phi \tilde\rho(\mathcal{J}_{\boldsymbol f}(\Phi))}{\Delta x} + \frac{\max_\Phi \tilde\rho(\boldsymbol{B}(\Phi))}{2\Delta x^2}\Big)^{-1} \tag{5.1}$$

with $C_{\rm cfl1} = 0.25$ and with estimates $\tilde\rho$ of the spectral radius of the corresponding matrices obtained from Theorems 2.1 and 2.2 for the polydisperse case and Theorem 2.3 and Lemma 2.4 for the traffic model. This CFL number has been empirically adjusted to be the largest multiple of 0.05 that yields an oscillation-free reference solution. The variable time step (5.1) with $C_{\rm cfl1} = 0.25$ has been used for the KT scheme in all the following tests.

We use the following time steps for the IMEX-RK schemes:

$$\Delta t = C_{\rm cfl2}\Delta x\big(\max_\Phi \rho(\mathcal{J}_{\boldsymbol f}(\Phi))\big)^{-1}, \tag{5.2}$$

where $\rho(\mathcal{J}_{\boldsymbol f}(\Phi))$ is computed along with the characteristic information needed for the convective part and $C_{\rm cfl2}$ is empirically obtained as the largest multiple of 0.05 that yields oscillation-free simulations with $M_{\rm ref}$ cells. These numbers are $C_{\rm cfl2} = 0.25$ for the scheme IMEX-RK(1,1,1) (3.9) in Examples 1 and 2 and $C_{\rm cfl2} = 0.1$ for Examples 3 and 4, whereas $C_{\rm cfl2} = 0.7$ for the methods IMEX-RK(2,2,2) (3.10) and IMEX-RK(3,4,3) (3.11), (3.12) in all examples. We mention that the scheme IMEX-RK(1,1,1) applied to fifth-order WENO (WENO5) spatial semidiscretizations should have a stability restriction related to that for the forward Euler method and WENO5. A modified von Neumann analysis carried out in [29] indicates that the CFL number of the schemes obtained by using Euler method to integrate semidiscretizations obtained by WENO5 have a stability restriction proportional to Δx^4. In our experiments we have not had to use such a small restriction, but we have had to reduce the Courant number considerably with respect to the other IMEX-RK methods.

5.1. Example 1: settling of a tridisperse suspension. We simulate the settling of a tridisperse ($N = 3$) suspension forming a compressible sediment. The mixture is described by the model functions (2.8), (2.3), (2.4) with $\phi_{\max} = 0.66$, $n_{\rm RZ} = 4.7$, $\sigma_0 = 180\,{\rm Pa}$, $\phi_{\rm c} = 0.2$, $k = 2$, $\mu_{\rm f} = 10^{-3}\,{\rm Pa\,s}$, $d = 1.19\times10^{-5}\,{\rm m}$, $\overline{\rho}_{\rm s} = 1800\,{\rm kg/m^3}$, and $g = 9.81\,{\rm m/s^2}$ [5]. The initial concentration is $\Phi_0 = (0.04, 0.04, 0.04)^{\rm T}$ in a vessel of height $K = 1{\rm m}$ with normalized squared particle sizes $\boldsymbol{\delta} = (1, 0.5, 0.25)^{\rm T}$.

For this model, according to (2.6), the coefficients are defined in terms of the function $\sigma_{\rm e}(\phi)$ and its derivative. The regularization mentioned in Section 4 is achieved by replacing $\sigma_{\rm e}(\phi)$ by a regularized smooth function $\sigma_{\rm e}(\phi;\varepsilon)$ such that $\sigma_{\rm e}(\phi;\varepsilon) \to \sigma_{\rm e}(\phi)$ for all ϕ and $\sigma'_{\rm e}(\phi;\varepsilon) \to \sigma'_{\rm e}(\phi)$ for all $\phi \neq \phi_{\rm c}$ as $\varepsilon \to 0$. Specifically, if $\sigma_{\rm e}$ satisfied (2.7), we choose

$$\sigma_{\rm e}(\phi;\varepsilon) = \sigma_{\rm e}(\phi)\exp\big(-\varepsilon/(\phi-\phi_{\rm c})^2\big), \quad \varepsilon > 0. \tag{5.3}$$

In Figure 5.1 we compare results obtained by schemes KT, IMEX-RK(1,1,1), IMEX-RK(2,2,2) and IMEX-RK(3,4,3). We observe good approximations for the IMEX-RK schemes compared with the KT scheme near $\phi_{\rm c}$ and no oscillations are observed at this scale. For solving the nonlinear system (3.7) that appears in the IMEX-RK formulation, we use Algorithm 4.1 where ε varies from $\varepsilon_0 = 10^{-4}$ to $\varepsilon_{\min} = 10^{-7}$ and ${\rm tol} = 10^{-8}$. In Figure 5.2 we display numerical approximations calculating the diffusion coefficient with (5.3) for different fixed values of ε. Note that for $\varepsilon =$

TABLE 5.1

Examples 1 and 4: maximum number of iterations $\nu_{\max}$ required by the NR method for solving (3.7), maximum number of reductions $k_{\max}$ of α in Algorithm 4.1, global average number of iterations $\bar{\nu}$, and global average number of reductions $\bar{k}$ of α required for two different discretizations (a) by IMEX-RK(2,2,2) for Example 1, (b) by IMEX-RK(3,4,3) for Example 4.

(a)

M	$\nu_{\max}$	$k_{\max}$	$\bar{\nu}$	$\bar{k}$
200	4	0	2.1	0
800	6	2	2.45	0.01

(b)

M	$\nu_{\max}$	$k_{\max}$	$\bar{\nu}$	$\bar{k}$
400	6	5	3.8	0.4
1600	9	7	4.4	0.5

TABLE 5.2

*Example 1: total approximate L^1 errors $e_{\text{tot}}(T)$ ("error"), multiplied by 10^{-5}; convergence rates (*cr*), and CPU times (*cpu*), at two simulated times T for the schemes KT and IMEX-RK(1,1,1) with $C_{\text{cfl1}} = C_{\text{cfl2}} = 0.25$, and the schemes IMEX-RK(2,2,2) and IMEX-RK(3,4,3) with $C_{\text{cfl2}} = 0.7$.*

		KT			IMEX-RK(1,1,1)			IMEX-RK(2,2,2)			IMEX-RK(3,4,3)		
T [s]	M	error	cr	cpu	error	cr	cpu [s]	error	cr	cpu [s]	error	cr	cpu [s]
4000	100	150.4	—	0.6	131.8	—	0.2	148.8	—	0.2	149.1	—	0.3
	200	75.7	0.99	4.7	62.7	1.07	0.9	73.4	1.02	0.7	74.0	0.98	1.2
	400	38.4	0.98	26.6	31.1	1.01	3.7	37.0	0.98	2.6	37.1	0.61	4.6
	800	20.8	0.88	289.1	18.1	0.78	14.6	20.0	0.89	9.9	19.9	1.04	19.2
	1600	11.3	0.88	2349.0	9.1	0.98	65.4	10.1	0.97	44.7	10.1	0.86	81.8
10000	100	141.1	—	2.4	139.5	—	0.6	140.5	—	0.5	139.5	—	0.8
	200	75.6	0.89	18.1	69.3	1.01	2.6	70.8	0.98	1.9	70.9	0.97	3.2
	400	40.2	0.91	101.6	44.9	6.24	10.0	46.9	0.61	6.9	47.2	0.61	12.4
	800	21.6	0.89	1103.0	21.4	1.07	40.1	22.7	1.04	27.1	22.1	1.09	49.7
	1600	12.6	0.78	9058.6	12.2	0.81	175.3	12.4	0.96	116.3	12.4	0.84	218.3

10^{-5}, we obtain a good approximation with respect to the reference solution and it is remarkable that for fixed $\varepsilon \leq 10^{-6}$, the NR method did not converge. On the other hand, the strategy of reduction of ε in Algorithm 4.1 succeeds for smaller $\varepsilon_{\min}$.

In Table 5.1 (a) we describe some details of the convergence history of the NR method to obtain a numerical approximation at simulated time $T = 10000$s using the IMEX-RK(2,2,2) scheme with $M = 200$ and $M = 800$ cells. Observe that for $M = 800$, for each fixed value of ε, the NR method required at most 6 iterations, but in general, only 2 or 3 iterations iterations were necessary. With respect to α, Algorithm 4.1 reduced this parameter twice, which means that the line search strategy was used at some point, but in general it was not necessary. It is worth pointing out that the FP iterative procedure (4.1) did not converge for $\varepsilon < 10^{-2}$.

Table 5.2 and Figure 5.3 show approximate L^1 total errors, convergence rates (cr) and CPU times (cpu) for Example 1. These approximate errors are computed as follows: Let us denote by $(\phi_{j,i}^M(t))_{j=1}^M$ and $(\phi_{l,i}^{\text{ref}}(t))_{l=1}^{M_{\text{ref}}}$ the numerical solution for the i-th component at time t calculated with M and M_{ref} cells, respectively. We use cubic interpolation from the reference grid to the M cells grid to compute $\widetilde{\phi}_{j,i}^{\text{ref}}(t)$ for $j = 1, \ldots, M$. We then calculate the approximate L^1 error in species i by

$$e_i(t) := \frac{1}{M} \sum_{j=1}^{M} \left| \widetilde{\phi}_{j,i}^{\text{ref}}(t) - \phi_{j,i}^M(t) \right|, \quad i = 1, \ldots, N.$$

We define the total approximate L^1 error at time t as $e_{\text{tot}}(t) := e_1(t) + \cdots + e_N(t)$.

As can be deduced from Table 5.2, the most efficient scheme is IMEX-RK(2,2,2): for the same resolution M the IMEX-RK(1,1,1) scheme has the smallest error, closely followed by the IMEX-RK(2,2,2), IMEX-RK(3,4,3) and KT schemes, in increasing

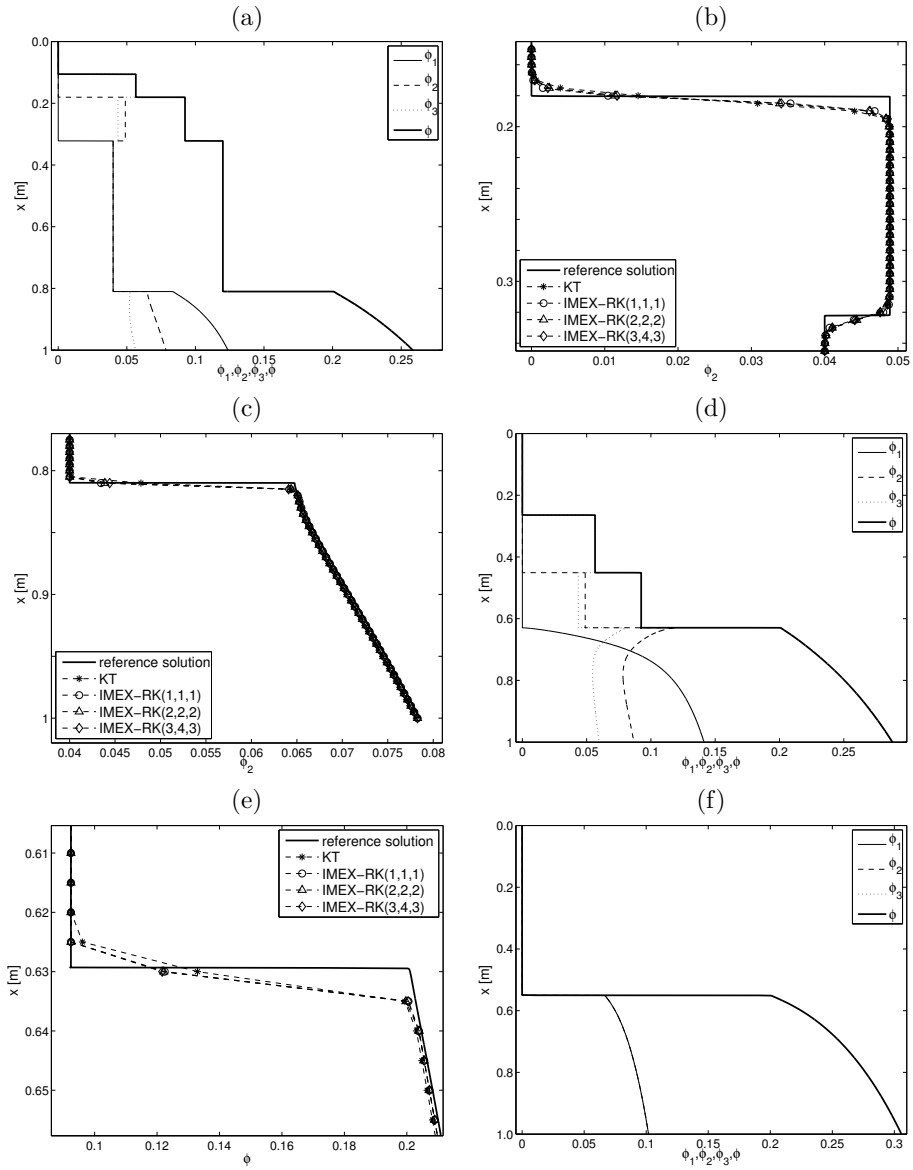

FIG. 5.1. *Example 1: (a) reference solution (KT scheme, $M = 12800$) at simulated time $T = 4000\,\mathrm{s}$, (b, c) enlarged view of solution by KT and IMEX-RK schemes with $M = 200$ at $T = 4000\,\mathrm{s}$, (d) reference solution at $T = 10000\,\mathrm{s}$, (e) enlarged view of solution by KT and IMEX-RK schemes with $M = 200$ at $T = 10000\,\mathrm{s}$, (f) reference solution at $T = 50000\,\mathrm{s}$.*

order with respect to error size; on the other hand, the CPU time of IMEX-RK(2,2,2) is the lowest, basically due to the increased CFL number with respect to the IMEX-RK(1,1,1) scheme and the smaller number of implicit stages with respect to the IMEX-RK(3,4,3) scheme. One can also deduce from Table 5.2 that the CPU time scales as $\mathcal{O}(M^2)$ for the IMEX schemes, whereas it scales as $\mathcal{O}(M^3)$ for the KT scheme. This implies a nearly fixed cost of the solution of nonlinear systems per time step and that the gap in CPU time increases with M. For instance, IMEX-RK(2,2,2) is about 60

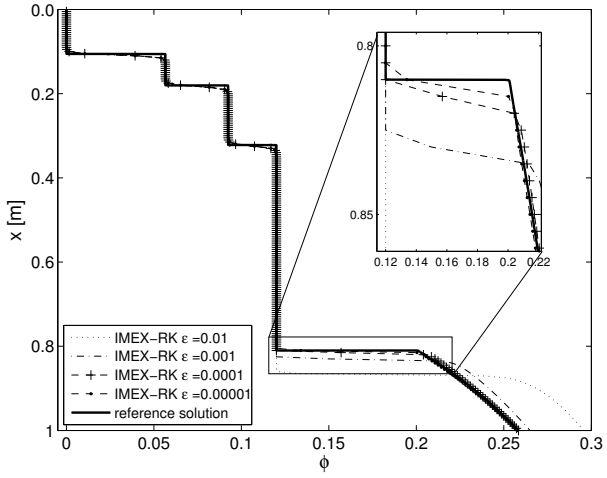

FIG. 5.2. *Example 1: numerical approximation by at simulated time $T = 4000s$ using a fixed ε value in the function* (5.3).

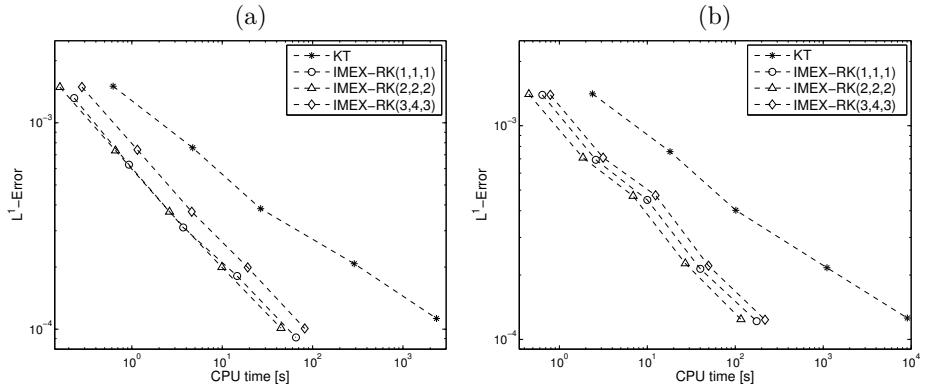

FIG. 5.3. *Example 1: total approximate L^1 errors versus CPU time for KT and IMEX-RK schemes at simulated times (a) $T = 4000$ s, (b) $T = 10000$ s. Here and in Figures 5.5, 5.8 and 5.10, for each scheme the interpolated symbols correspond to different values of M.*

times faster than the KT scheme for a resolution of $M = 1600$ cells.

We note that a careful observation of CPU times of the same scheme and resolution at different simulated times yields that the CPU time is not proportional to the simulated time. This is due the variable time stepping in formulas (5.1) and (5.2) and to the fact that the spectral radius of the Jacobian of the fluxes and the diffusion matrix is smaller at the early stages of the simulation (in fact, the diffusion matrix may be null in a noticeable period of time) so the time steps may be larger at the beginning of the simulation.

5.2. Example 2. We now simulate the settling of a polydisperse suspension of $N = 8$ species forming a compressible sediment with a sufficiently smooth diffusion coefficient, thus allowing us to use directly the FP (4.1) and NR nonlinear solvers without resorting to Algorithm 4.1, since, in this case, there is no need to

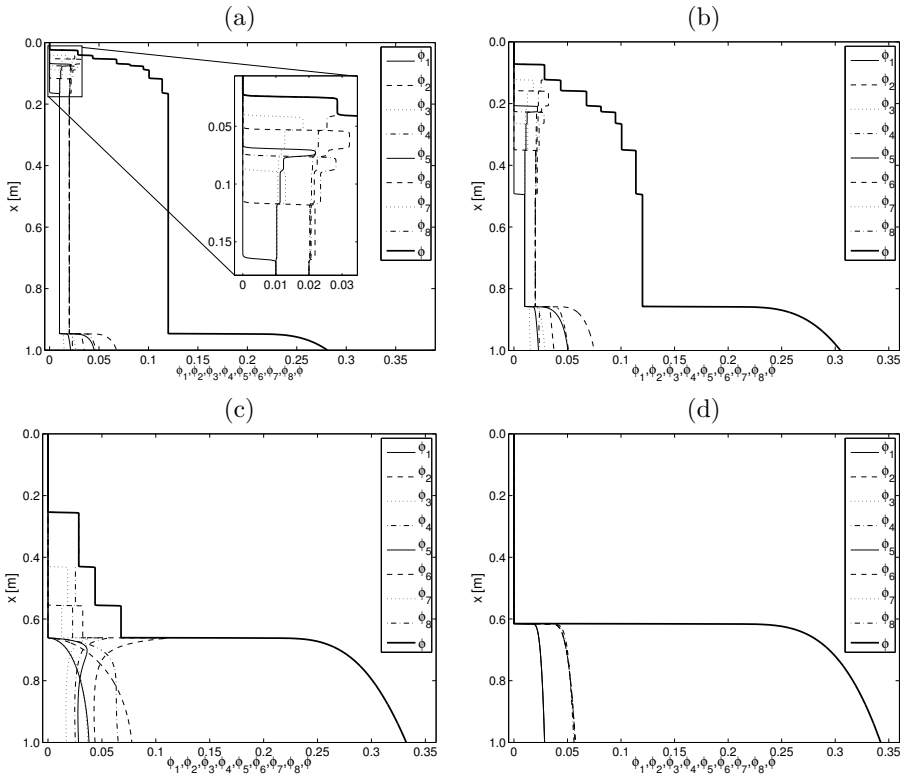

FIG. 5.4. *Example 2: numerical solution obtained by scheme IMEX-RK(3,4,3)-N with* $M = 1600$ *cells at simulated times (a)* $T = 2000\,\mathrm{s}$ *(including enlarged view of spreading suspension-supernate transition zone), (b)* $T = 6000\,\mathrm{s}$*, (c)* $T = 21000\,\mathrm{s}$ *and (d)* $T = 120000\,\mathrm{s}$.

TABLE 5.3
Example 2: Initial conditions ϕ_i^0*, normalized squared particle sizes* δ_i.

i	1	2	3	4	5	6	7	8
$\phi_i^0[10^{-2}]$	1.0	2.0	1.0	2.0	1.0	2.0	1.0	2.0
δ_i	1.00	0.70	0.50	0.42	0.36	0.26	0.18	0.10

regularize the diffusion coefficients. We denote by IMEX-RK-NR and IMEX-RK-FP the corresponding IMEX-RK schemes with the NR method and the FP algorithm, respectively. Figure 5.4 shows the numerical solution obtained with IMEX-RK(3,4,3)-NR with $M = 1600$ cells at several times. In Table 5.4 and Figure 5.5, we display total approximate L^1 errors and CPU times for the different schemes at different discretizations. In both cases we observe that the IMEX-RK scheme is faster than the KT scheme, and that the NR version of each scheme is faster than the corresponding FP version, even when the number of equations N is large. A solution for the nonlinear system (3.7) at each time step is obtained when $\|\boldsymbol{u}^{(\nu+1)} - \boldsymbol{u}^{(\nu)}\| < 10^{-8}$.

With respect to efficiency, Table 5.4 leads to conclusions similar those drawn in Example 1. Here the errors obtained with the IMEX schemes are roughly half those obtained with the KT scheme, whereas the CPU time speedup reaches a factor of about 60 if we compare, for instance, the CPU times of KT and IMEX-RK(1,1,1)-NR for $M = 1600$ and $T = 6000\,\mathrm{s}$.

TABLE 5.4

Example 2: total approximate L^1 errors (in short, "error"), multiplied by 10^{-5}; convergence rates (cr), and CPU times (in seconds), at times $T = 6000\,\mathrm{s}$ and $T = 21000\,\mathrm{s}$ for KT and IMEX-RK(1,1,1) schemes with CFL condition $C_{\mathrm{cfl1}} = C_{\mathrm{cfl2}} = 0.25$, IMEX-RK(2,2,2) and IMEX-RK(3,4,3) with CFL condition $C_{\mathrm{cfl2}} = 0.7$. The nonlinear system (3.7) is solved either by the NR or the FP method (versions "-NR" and "-FP").

			KT		IMEX-RK(1,1,1)-NR			IMEX-RK(2,2,2)-NR			IMEX-RK(3,4,3)-NR		
T [s]	M	error	cr	cpu [s]	error	cr	cpu [s]	error	cr	cpu [s]	error	cr	cpu
	100	444.4	—	1.4	257.2	—	0.7	280.4	—	0.8	281.4	—	1.0
	200	257.5	0.80	12.0	144.7	0.82	3.0	159.2	0.81	3.3	169.2	0.73	4.1
6000	400	118.2	1.12	96.0	57.7	1.32	11.8	65.4	1.22	13.5	70.4	1.26	16.5
	800	54.7	1.11	836.1	27.1	1.09	52.4	30.7	1.08	54.2	31.7	1.14	71.2
	1600	29.3	0.90	6327.7	15.3	0.81	211.4	15.8	0.95	218.0	16.8	0.91	300.8
					IMEX-RK(1,1,1)-FP			IMEX-RK(2,2,2)-FP			IMEX-RK(3,4,3)-FP		
T [s]	M				error	cr	cpu [s]	error	cr	cpu [s]	error	cr	cpu [s]
	100				257.1	—	2.0	280.4	—	1.3	280.8	—	2.4
	200				144.7	0.82	8.5	159.2	0.81	5.5	159.3	0.82	10.1
6000	400				57.7	1.32	33.7	65.4	1.28	22.5	65.3	1.28	43.1
	800				27.1	1.09	138.8	30.7	1.09	95.3	30.8	1.08	169.7
	1600				15.3	0.81	594.2	16.8	0.86	413.3	16.8	0.88	741.1
			KT		IMEX-RK(1,1,1)-NR			IMEX-RK(2,2,2)-NR			IMEX-RK(3,4,3)-NR		
T [s]	M	error	cr	cpu [s]	error	cr	cpu [s]	error	cr	cpu [s]	error	cr	cpu [s]
	100	431.8	—	10.3	224.8	—	2.8	229.7	—	2.9	229.9	—	3.4
	200	230.2	0.90	90.4	118.6	0.92	11.0	121.2	0.92	11.7	121.2	0.92	13.3
21000	400	125.6	0.87	721.6	64.3	0.88	44.0	65.7	0.88	46.7	65.7	0.88	52.7
	800	67.9	0.88	5885.5	40.4	0.66	189.3	41.1	0.68	198.7	41.1	0.67	211.1
	1600	37.6	0.84	36809.6	21.4	0.91	682.0	21.7	0.92	756.3	21.7	0.91	894.3
					IMEX-RK(1,1,1)-FP			IMEX-RK(2,2,2)-FP			IMEX-RK(3,4,3)-FP		
T [s]	M				error	cr	cpu [s]	error	cr	cpu [s]	error	cr	cpu [s]
	100				224.8	—	7.1	229.7	—	4.3	229.9	—	7.7
	200				118.6	0.92	29.3	121.2	0.92	17.8	121.2	0.92	32.3
21000	400				64.4	0.88	125.6	65.7	0.88	73.5	65.7	0.88	133.0
	800				40.6	0.66	481.4	41.1	0.67	310.0	41.1	0.67	553.3
	1600				22.7	0.83	1946.4	23.3	0.81	1331.4	21.7	0.91	2403.1

A comparison of the entries corresponding to the NR versions of the IMEX-RK schemes with those of the FP versions in Table 5.4 indicates the superior efficiency of the NR method compared with the FP iterative solver. This is basically explained by a lower convergence rate of the latter with respect to the former, which yields an increased number of iterations with a similar computational cost per iteration.

5.3. Examples 3 and 4: diffusively corrected kinematic traffic model. We consider a circular road and a number N of driver classes associated with velocities $v_i^{\max} > v_j^{\max}$ for $i < j$. If ρ_i denotes the number of cars of species i per mile, and $\rho_{\max}$ is the maximal "bumper-to-bumper" number of cars per mile, we define $\phi_i := \rho_i/\rho_{\max}$. To make results comparable with those of [10], we employ the Dick-Greenberg model [14, 22] $V(\phi) = V_{\mathrm{DG}}(\phi) = \min\{1, -C\ln\phi\}$, and choose (as in [10, 30, 31]) $C = \mathrm{e}/7 \approx 0.38833$ so that

$$\begin{cases} V(\phi) = 1,\ V'(\phi) = 0 & \text{for } 0 \le \phi \le \phi_{\mathrm{c}} = \exp(-1/C) \approx 0.076142, \\ V(\phi) = -C\ln\phi,\ V'(\phi) = -C/\phi & \text{for } \phi_{\mathrm{c}} < \phi < 1. \end{cases} \tag{5.4}$$

We equip class 1 with exactly the same properties as the vehicles considered in [10], and therefore set $\tau = 2\,\mathrm{s} = 0.000\bar{5}\,\mathrm{h}$. We choose all anticipation lengths $L_i = L = 0.05\,\mathrm{mi}$ and all reaction times $\tau_i = \tau$, $i = 1, \ldots, N$ in such a way that (2.20) holds

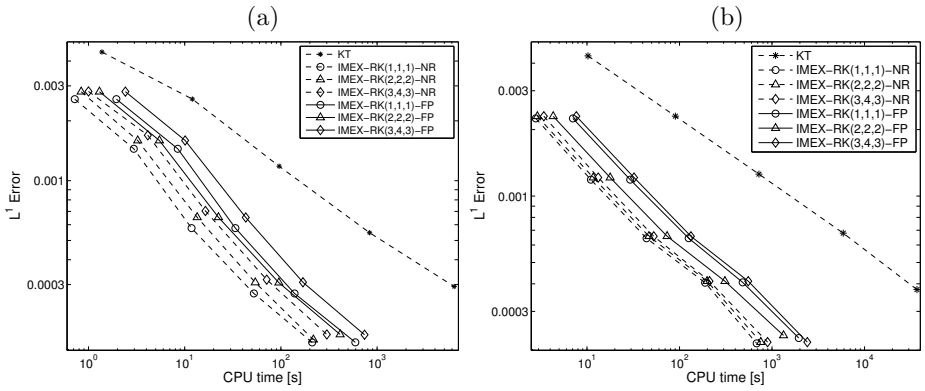

FIG. 5.5. *Example 2: total approximate L^1 errors versus CPU time for KT, IMEX-RK-N and IMEX-RK-Fp schemes at simulated times (a) $T = 6000\,\mathrm{s}$, (b) $T = 21000\,\mathrm{s}$.*

with $\phi_{\max} = 1$, i.e.,

$$\tau \le \min_{0\le\phi\le 1}\left(-\frac{L(\phi)}{\phi V'(\phi) v_1^{\max}}\right) = \frac{L}{C v_1^{\max}} = \frac{7\cdot 0.05\,\mathrm{mi}}{\mathrm{e}\cdot 70\mathrm{mi/h}} \approx 0.00184\,\mathrm{h} = 6.622\,\mathrm{s}.$$

We easily see that in this case

$$C_2 = \tau^2 (V(\phi))^2 \sum_{\substack{i,j=1\\ i<j}}^{N} \phi_i v_i^{\max} \phi_j v_j^{\max} (v_j^{\max} - v_i^{\max})^2 \ge 0.$$

For this model, according to (2.13), the coefficients depend on $V(\phi)$ and its derivative. The regularization mentioned in Section 4 is achieved by replacing $V(\phi)$ by

$$V(\phi;\varepsilon) = 1 + (V(\phi) - 1)\exp\bigl(-\varepsilon/(\phi - \phi_{\mathrm{c}})^2\bigr), \quad \varepsilon > 0. \tag{5.5}$$

To be definite, we study $N = 3$ vehicle classes with $v_1^{\max} = 70\,\mathrm{mi/h}$, $v_2^{\max} = 50\,\mathrm{mi/h}$ and $v_3^{\max} = 30\,\mathrm{mi/h}$ on a circular roadway with length $K = 4\mathrm{mi}$, i.e., we use periodic boundary conditions. The initial density distribution is given by an isolated platoon of maximum global density ρ_0, $\Phi_0(x,0) = p(x-1)\rho_0(0.25, 0.4, 0.35)^{\mathrm{T}}$, where

$$p(x) = \begin{cases} 10x & \text{for } 0 < x \le 0.1, \\ 1 & \text{for } 0.1 < x \le 0.9, \end{cases} \qquad \begin{cases} -10(x-1) & \text{for } 0.9 < x \le 1, \\ 0 & \text{otherwise,} \end{cases}$$

and we choose $\rho_0 = 0.45$ and $\rho_0 = 0.25$ in Examples 3 and 4, respectively.

Figure 5.6 shows the time evolution with IMEX-RK(3,4,3) and $M = 1600$ cells of the initial density platoon for Example 3. The average density exceeds ϕ_{c}, i.e., the traffic is relatively dense. We observe that the numerical solution evolves to a stationary solution, which must lie in the parabolic region. In this test the velocity function (5.4) is regularized by (5.5) as in Example 1. Algorithm 4.1 was used with ε varying from $\varepsilon_0 = 10^{-3}$ to $\varepsilon_{\min} = 10^{-6}$ and $\mathrm{tol} = 10^{-8}$. Previous numerical tests indicated that $\varepsilon_{\min} = 10^{-6}$ was sufficient to obtain good approximations.

In Figure 5.7 we compare the results obtained by the KT and IMEX-RK schemes. Plotted areas correspond to regions where the diffusive term acts. We observe that the IMEX-RK schemes approximate adequately the reference solution. In Table 5.5 and

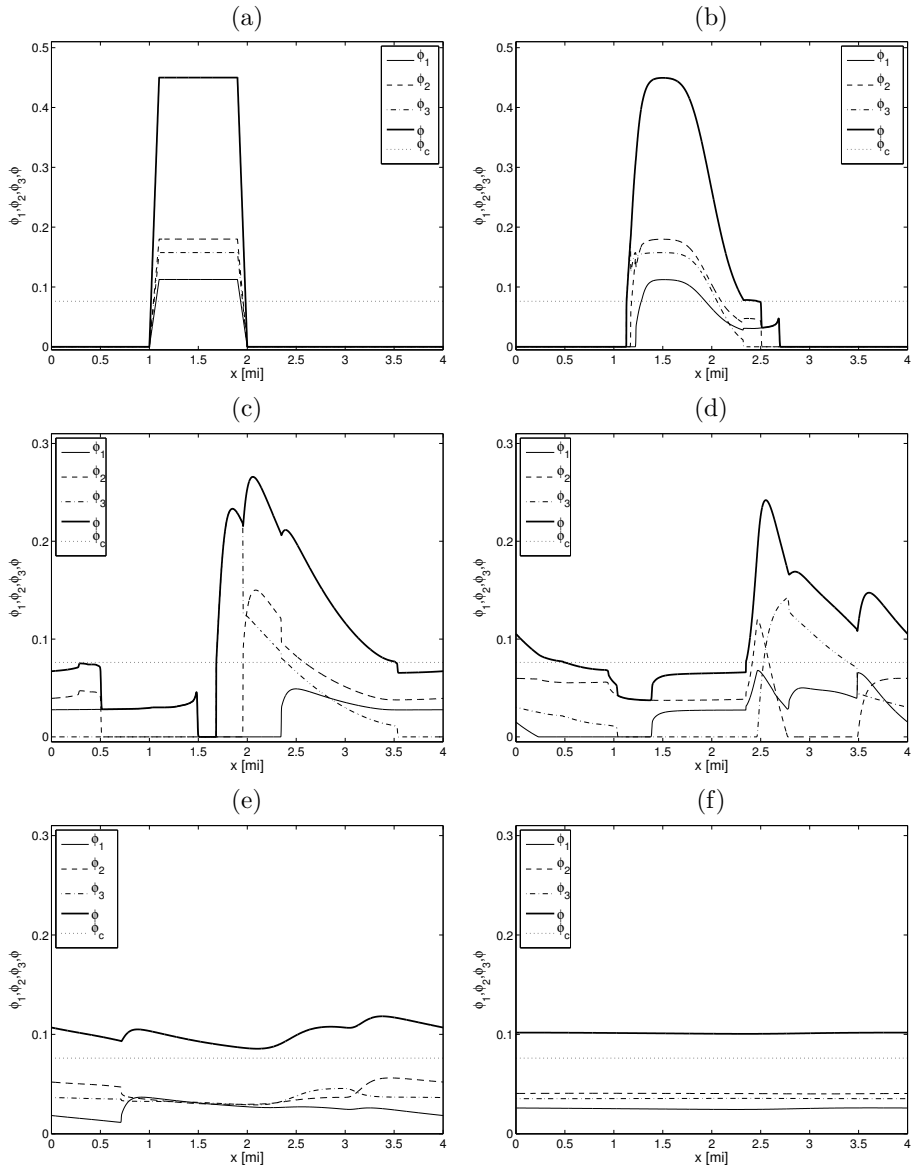

FIG. 5.6. *Example 3: numerical solution obtained with scheme IMEX-RK(3,4,3) with* $M = 1600$ *at simulated times (a)* $T = 0.0\,\mathrm{h}$ *(initial datum), (b)* $T = 0.01\,\mathrm{h}$*, (c)* $T = 0.05\,\mathrm{h}$*, (d)* $T = 0.1\,\mathrm{h}$*, (e)* $T = 0.5\,\mathrm{h}$ *and (f)* $T = 5.0\,\mathrm{h}$.

Figure 5.8 we display the history of total approximate L^1 errors and CPU times for Example 3. From Figure 5.8 we infer that IMEX-RK(2,2,2) and IMEX-RK(3,4,3) are always more efficient than the KT scheme, with speedup factors above 10. However, for small resolutions, the IMEX-RK(1,1,1) is penalized by the CFL reduction and, for instance, it is less efficient than the KT scheme for $M = 200$.

In Table 5.1 (b) we describe some details of the convergence history of the NR method to obtain numerical approximations at simulated time $T = 0.2$h using IMEX-RK(3,4,3) scheme with $M = 400$ and $M = 1600$ subintervals. Observe that for

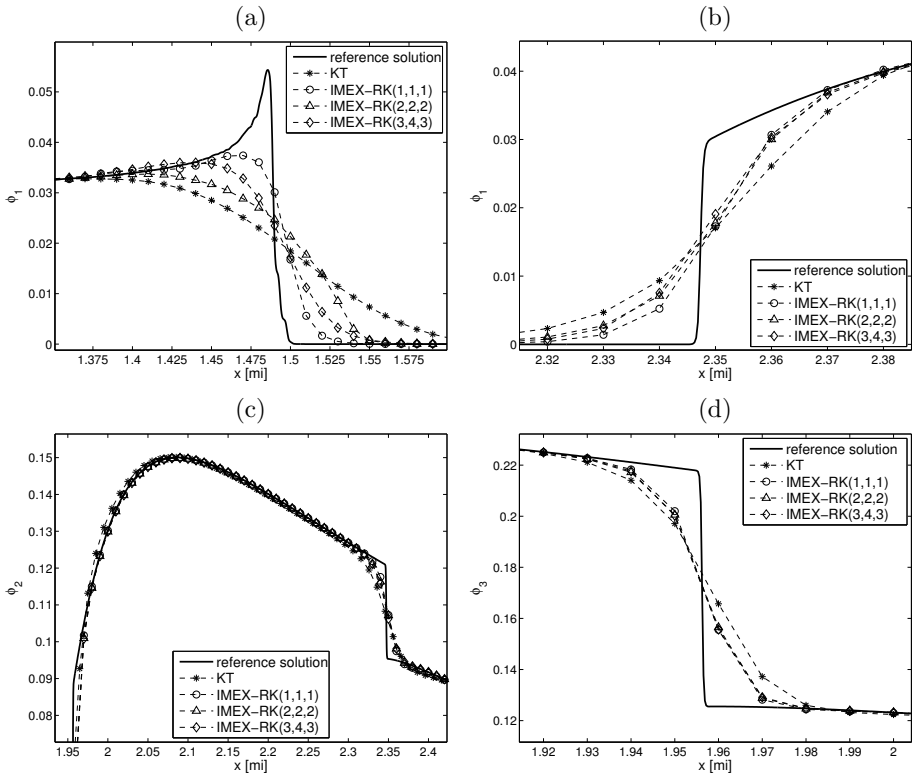

FIG. 5.7. *Example 3: (a) reference solution (scheme KT, $M_{\rm ref} = 12800$), (b, c, d) enlarged views of reference solution and numerical solutions for individual species for KT and IMEX-RK schemes with $M = 400$, at simulated time $T = 0.2$ h.*

TABLE 5.5
Example 3: total approximate L^1 errors multiplied by 10^{-5}, convergence rates and CPU times at time T for scheme KT with $C_{\rm cfl1} = 0.25$, scheme IMEX-RK(1,1,1) with $C_{\rm cfl2} = 0.1$, and schemes IMEX-RK(2,2,2) and IMEX-RK(3,4,3) with $C_{\rm cfl2} = 0.7$.

		KT			IMEX-RK(1,1,1)			IMEX-RK(2,2,2)			IMEX-RK(3,4,3)		
T [h]	M	error	cr	cpu [s]	error	cr	cpu [s]	error	cr	cpu [s]	error	cr	cpu [s]
	200	305.7	—	1.4	302.1	—	2.4	321.3	—	0.6	305.8	—	1.1
	400	172.4	0.82	10.4	170.1	0.82	9.6	183.5	0.80	2.7	170.6	0.84	4.8
0.05	800	88.4	0.96	78.6	88.6	0.94	42.2	97.2	0.91	12.5	83.7	1.02	22.4
	1600	42.8	1.04	592.5	44.2	1.00	181.8	49.9	0.96	58.9	38.9	1.10	102.1
	3200	22.8	0.90	4704.5	25.5	0.80	797.2	25.5	0.96	263.9	20.0	0.96	475.6
	200	343.2	—	5.3	279.8	—	15.5	188.7	—	4.2	167.6	—	6.8
	400	165.7	1.04	40.9	145.9	0.93	73.3	91.2	1.04	16.8	82.6	1.02	28.2
0.25	800	74.5	1.15	324.1	78.0	0.90	270.3	38.2	1.25	76.0	31.4	1.39	136.0
	1600	37.2	0.99	2022.1	36.9	1.07	1016.8	19.6	0.95	326.2	15.8	0.98	549.9
	3200	19.4	0.94	14965.5	20.5	0.84	4155.6	10.3	0.92	1376.8	7.7	1.02	2482.9

$M = 1600$ and each fixed value of ε, the NR method required at most 9 iterations, but in average, only 4 or 5 iterations were necessary. With respect to α, at some point Algorithm 4.1 reduced it seven times but, in general, no more that one reduction was necessary.

In Example 4 we choose $\rho_0 = 0.25$ so that the average density is below $\phi_{\rm c}$. This case does not evolve into a stationary solution. In Figure 5.9 we compare results ob-

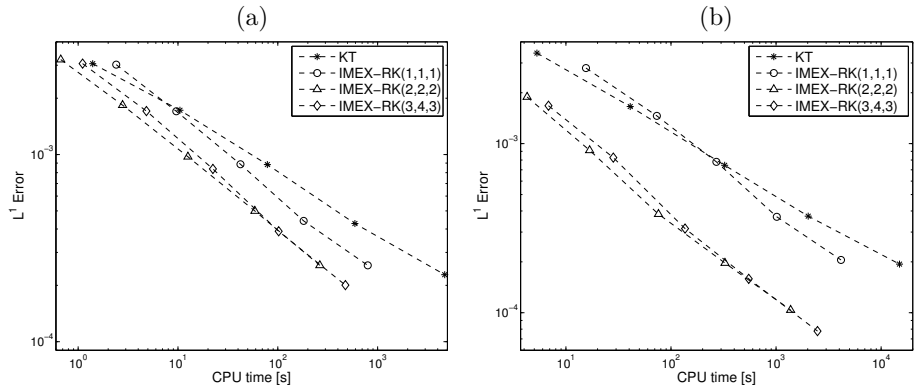

FIG. 5.8. *Example 3: total approximate L^1 errors versus CPU time for KT and IMEX-RK schemes at simulated times (a) $T = 0.05\,\mathrm{h}$, (b) $T = 0.25\,\mathrm{h}$.*

tained by the KT, IMEX-RK(1,1,1), IMEX-RK(2,2,2) and IMEX-RK(3,4,3) schemes at simulated time $T = 0.2$h with respect to the reference solution. Numerical approximations are computed with IMEX-RK(3,4,3) and $M = 1600$ cells. We observe that the IMEX-RK schemes approximate adequately the reference solution.

In Table 5.6 and Figure 5.10, we display total approximate L^1 errors and CPU times for Example 4. We infer that IMEX-RK(2,2,2) and IMEX-RK(3,4,3) are always more efficient than the KT scheme. We observe the same trends as those mentioned for the previous setup.

TABLE 5.6

Example 4: total approximate L^1 total errors, multiplied by 10^{-5}, convergence rates and CPU times for KT scheme with $C_{\mathrm{cfl1}} = 0.25$, scheme IMEX-RK(1,1,1) with $C_{\mathrm{cfl2}} = 0.1$, and schemes IMEX-RK(2,2,2) and IMEX-RK(3,4,3) with $C_{\mathrm{cfl2}} = 0.7$.

		KT			IMEX-RK(1,1,1)			IMEX-RK(2,2,2)			IMEX-RK(3,4,3)		
T [h]	M	error	cr	cpu [s]	error	cr	cpu [s]	error	cr	cpu [s]	error	cr	cpu [s]
	200	283.8	—	0.8	294.8	—	2.5	291.8	—	0.7	261.7	—	1.2
	400	170.9	0.71	6.8	150.4	0.97	10.1	180.9	0.69	2.9	167.7	0.65	4.9
0.06	800	96.9	0.81	56.9	82.9	0.85	41.8	98.9	0.87	12.6	88.5	0.92	21.3
	1600	48.4	1.01	307.9	45.5	0.86	166.5	49.4	1.01	53.5	45.3	0.96	85.4
	3200	25.1	0.94	2660.1	26.2	0.79	874.4	25.1	0.97	215.1	24.1	0.90	326.2
	200	186.0	—	3.0	183.3	—	8.8	190.9	—	2.4	155.5	—	3.9
	400	93.6	0.99	20.5	95.2	0.94	34.9	97.2	0.97	9.6	73.6	1.07	16.1
0.20	800	49.3	0.92	157.4	50.1	0.92	138.3	49.3	0.98	41.2	34.6	1.08	69.0
	1600	25.0	0.97	1367.8	27.3	0.87	546.3	22.0	1.16	175.3	15.2	1.18	302.7
	3200	13.3	0.90	10261.1	14.4	0.92	2309.2	11.3	0.95	714.3	7.25	1.06	1246.1

6. Conclusions. Some kinematic models can be enriched with nonlinear, nonsmooth and strongly degenerate diffusive terms to account for certain additional features. Their long term fine simulations with explicit schemes is limited by the typical parabolic time step restriction, but implicit-explicit Runge-Kutta schemes can overcome this burden. We have shown why lagged diffusivity solvers for the nonlinear systems that appear in this IMEX formulation do not work for vanishing smoothness regularizations of the diffusion coefficients whereas a smart solving strategy based on the Newton-Raphson's method can be efficiently applied for this purpose. The speedup of these IMEX methods with respect to the Kurganov-Tadmor (explicit)

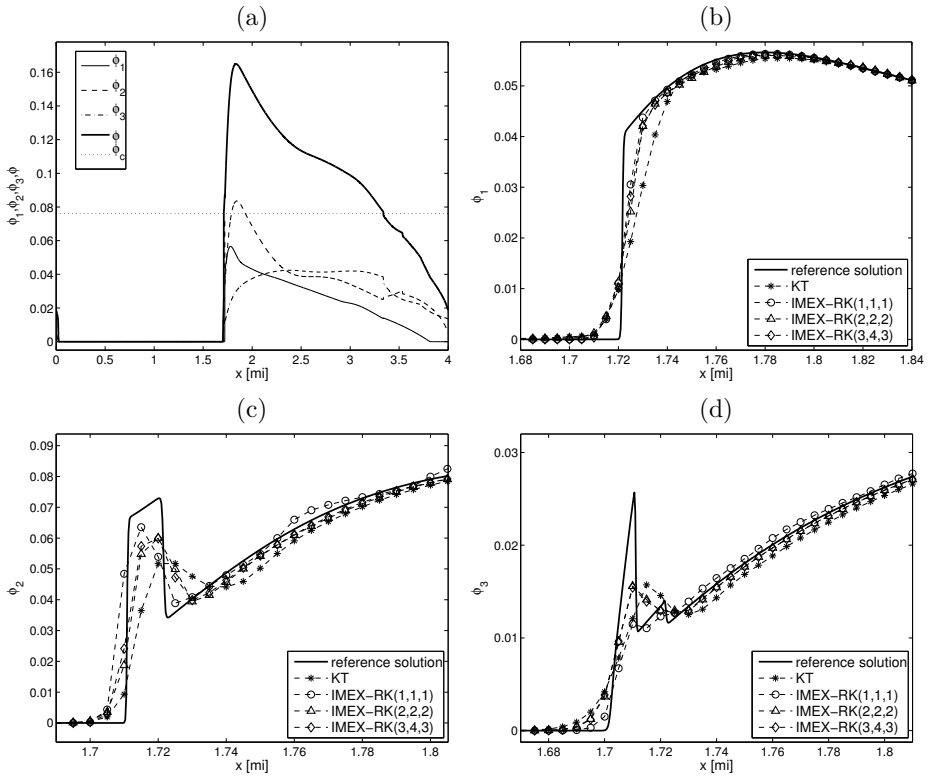

FIG. 5.9. *Example 4: (a) reference solution (scheme KT, $M_{\mathrm{ref}} = 12800$), (b, c, d) enlarged views of reference solution and numerical solutions for individual species for KT and IMEX-RK schemes with $M = 800$, at simulated time $T = 0.2\,\mathrm{h}$.*

scheme is computed for some selected tests and shown to be at least an order of magnitude for moderate spatial resolutions.

The limitations of this approach stem from the fact that a regularization of the diffusion coefficients has to be selected and there is a tradeoff between the fidelity to the original coefficients and computational time. Nevertheless, we stress that the proposed regularizations do not change the strong degeneracy of the diffusion.

In this work we have considered constant reaction times and anticipation lengths for all driver classes. We plan to investigate plausible conditions on those parameters to ensure the stability of the solutions of the models.

Acknowledgments. R. Bürger acknowledges partial support by Fondecyt project 1090456, BASAL project CMM, Universidad de Chile and Centro de Investigación en Ingeniería Matemática ($\mathrm{CI}^2\mathrm{MA}$), Universidad de Concepción, and CONICYT project Anillo ACT1118 (ANANUM). P. Mulet is partially supported by Spanish MCINN MTM2011-22741. L.M. Villada is supported by MECESUP project UCO0713.

REFERENCES

[1] A. Abeynaike, A.J. Sederman, Y. Khan, M.L. Johns, J.F. Davidson, and M.R. Mackley, *The experimental measurement and modelling of sedimentation and creaming for glycerol/biodiesel droplet dispersions*, Chem. Eng. Sci., 79 (2012), pp. 125–137.

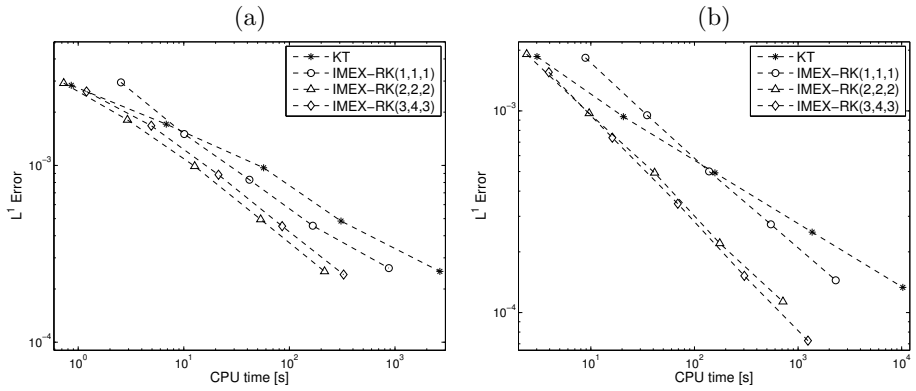

FIG. 5.10. *Example 4: total approximate L^1 errors versus CPU time for KT and IMEX-RK schemes at simulated times (a) $T = 0.06\,\mathrm{h}$, (b) $T = 0.2\,\mathrm{h}$.*

[2] J. ANDERSON, *A secular equation for the eigenvalues of a diagonal matrix perturbation*, Lin. Alg. Appl., 246 (1996), pp. 49–70.

[3] U. ASCHER, S. RUUTH, AND J. SPITERI, *Implicit-explicit Runge-Kutta methods for time dependent partial differential equations,* Appl. Numer. Math., 25 (1997), pp. 151–167.

[4] S. BENZONI-GAVAGE AND R.M. COLOMBO, *An n-populations model for traffic flow*, Eur. J. Appl. Math., 14 (2003), pp. 587–612.

[5] S. BERRES, R. BÜRGER, K.H. KARLSEN, AND E.M. TORY, *Strongly degenerate parabolic-hyperbolic systems modeling polydisperse sedimentation with compression*, SIAM J. Appl. Math., 64 (2003), pp. 41–80.

[6] S. BOSCARINO, L. PARESCHI, AND G. RUSSO, *Implicit-explicit Runge-Kutta schemes for hyperbolic systems and kinetic equations in the diffusion limit*, SIAM J. Sci. Comput., to appear.

[7] S. BOSCARINO AND G. RUSSO, *On a class of uniformly accurate IMEX Runge-Kutta schemes and applications to hyperbolic systems with relaxation*, SIAM J. Sci. Comput., 31 (2009), pp. 1926–1945.

[8] R. BÜRGER, R. DONAT, P. MULET, AND C.A. VEGA, *Hyperbolicity analysis of polydisperse sedimentation models via a secular equation for the flux Jacobian*, SIAM J. Appl. Math., 70 (2010), pp. 2186–2213.

[9] R. BÜRGER, R. DONAT, P. MULET, AND C.A. VEGA, *On the implementation of WENO schemes for a class of polydisperse sedimentation models*, J. Comput. Phys., 230 (2011), pp. 2322–2344.

[10] R. BÜRGER AND K.H. KARLSEN, *On a diffusively corrected kinematic-wave traffic flow model with changing road surface conditions*, Math. Models Methods Appl. Sci., 13 (2003), pp. 1767–1799.

[11] M. CROUZEIX, *Une méthode multipas implicite-explicite pour l'approximation des équations d'évolution paraboliques*, Numer. Math., 35 (1980), pp. 257–276.

[12] T. F. CHAN, G. H. GOLUB, AND P. MULET, *A nonlinear primal-dual method for total variation-based image restoration*, SIAM J. Sci. Comput., 20 (1999), pp. 1964–1977.

[13] J.E. DENNIS JR. AND R.B. SCHNABEL, *Numerical Methods for Unconstrained Optimization and Nonlinear Equations*, Classics in Applied Mathematics vol. 16, SIAM, 1996.

[14] A.C. DICK, *Speed/flow relationships within an urban area*, Traffic Engrg. Control, 8 (1996), pp. 393–396.

[15] R. DONAT AND I. HIGUERAS, *On stability issues for IMEX schemes applied to 1D scalar hyperbolic equations with stiff reaction terms*, Math. Comp., 80 (2011), pp. 2097–2126.

[16] R. DONAT AND P. MULET, *Characteristic-based schemes for multi-class Lighthill-Whitham-Richards traffic models*, J. Sci. Comput., 37 (2008), pp. 233–250.

[17] R. DONAT AND P. MULET, *A secular equation for the Jacobian matrix of certain multi-species kinematic flow models*, Numer. Methods Partial Differential Equations, 26 (2010), pp. 159–175.

[18] R. DORRELL, A.J. HOGG, E.J. SUMNER, AND P.J. TALLING, *The structure of the deposit produced by sedimentation of polydisperse suspensions*, J. Geophys. Res., 116 (2011), paper F01024.

[19] T. Frising, C. Noïk, and C. Dalmazzone, *The liquid/liquid sedimentation process: from droplet coalescence to technologically enhanced water/oil emulsion gravity separators: a review*, J. Disp. Sci. Technol., 27 (2006), pp. 1035–1057.
[20] S. Gottlieb and C.-W. Shu, *Total variation diminishing Runge-Kutta schemes*, Math. Comp., 67 (1998), pp. 73–85.
[21] S. Gottlieb, C.-W. Shu, and E. Tadmor, *Strong stability-preserving high-order time discretization methods*, SIAM Rev., 43 (2001), pp. 89–112.
[22] H. Greenberg, *An analysis of traffic flow*, Oper. Res., 7 (1979), pp. 79–85.
[23] G.S. Jiang and C.-W. Shu, *Efficient implementation of weighted ENO schemes*, J. Comput. Phys., 126 (1996), pp. 202–228.
[24] A. Kurganov and E. Tadmor, *New high-resolution central schemes for nonlinear conservation laws and convection-diffusion equations*, J. Comput. Phys., 160 (2000), pp. 241–282.
[25] M.J. Lighthill and G.B. Whitham, *On kinematic waves: II. A theory of traffic flow on long crowded roads*, Proc. Royal Soc. A, 229 (1955), pp. 317–345.
[26] X.-D. Liu, S. Osher, and T. Chan, *Weighted essentially non-oscillatory schemes*, J. Comput. Phys., 115 (1994), pp. 200–212.
[27] M.J. Lockett and K.S. Bassoon, *Sedimentation of binary particle mixtures*, Powder Technol., 24 (1979), pp. 1–7.
[28] J.H. Masliyah, *Hindered settling in a multiple-species particle system*, Chem. Engrg. Sci., 34 (1979), pp. 1166–1168.
[29] M. Motamed, C.B. Macdonald, and S.J. Ruuth, *On the linear stability of the fifth-order WENO discretization*, J. Sci. Comput., 47 (2011), pp. 127–149.
[30] P. Nelson, *Synchronized traffic flow from a modified Lighthill-Whitham model*, Phys. Rev. E, 61 (2000), pp. R6052–R6055.
[31] P. Nelson, *Traveling-wave solution of the diffusively corrected kinematic-wave model*, Math. Comp. Modelling, 35 (2002), pp. 561–579.
[32] D. Ngoduy, *Multiclass first-order traffic model using stochastic fundamental diagrams*, Transportmetrica, 7 (2011), pp. 111–125.
[33] D. Ngoduy and C. Tampere, *Macroscopic effects of reaction time on traffic flow characteristics*, Phys. Scr., 80 (2009), paper 025802 (8pp).
[34] L. Pareschi and G. Russo, *Implicit-Explicit Runge-Kutta schemes and applications to hyperbolic systems with relaxation,* J. Sci. Comput., 25 (2005), pp. 129-155.
[35] P.I. Richards, *Shock waves on the highway*, Oper. Res., 4 (1956), pp. 42–51.
[36] J.F. Richardson and W.N. Zaki, *Sedimentation and fluidization: Part I*, Trans. Instn. Chem. Engrs. (London), 32 (1954), pp. 35–53.
[37] F. Rosso and G. Sona, *Gravity-driven separation of oil-water dispersions*, Adv. Math. Sci. Appl., 11 (2001), pp. 127–151.
[38] C.-W. Shu, *Essentially non-oscillatory and weighted essentially non-oscillatory schemes for hyperbolic conservation laws.* In: B. Cockburn, C. Johnson, C.-W. Shu, and E. Tadmor, *Advanced Numerical Approximation of Nonlinear Hyperbolic Equations* (A. Quarteroni, Ed.), Lecture Notes in Mathematics vol. 1697, Springer-Verlag, Berlin (1998), pp. 325–432.
[39] C.-W. Shu, *High order weighted essentially nonoscillatory schemes for convection dominated problems*, SIAM Rev., 51 (2009), pp. 82–126.
[40] C.-W. Shu and S. Osher, *Efficient implementation of essentially non-oscilatory shock capturing schemes*, J. Comput. Phys., 77 (1988), pp. 439–471.
[41] K. Stamatakis and C. Tien, *Batch sedimentation calculations—the effect of compressible sediment*, Powder Technol., 72 (1992), pp. 227–240.
[42] G.C.K. Wong and S.C. Wong, *A multi-class traffic flow model—an extension of LWR model with heterogeneous drivers*, Transp. Res. A, 36 (2002), pp. 827–841.
[43] B. Xue and Y. Sun, *Modeling of sedimentation of polydisperse spherical beads with a broad size distribution*, Chem. Engrg. Sci., 58 (2003), pp. 1531–1543.
[44] A. Zeidan, S. Rohani, A. Bassi, and P. Whiting, *Review and comparison of solids settling velocity models*, Rev. Chem. Eng., 19 (2003), pp. 473–530.
[45] M. Zhang, C.-W. Shu, G.C.K. Wong, and S.C. Wong, *A weighted essentially non-oscillatory numerical scheme for a multi-class Lighthill-Whitham-Richards traffic flow model*, J. Comput. Phys., 191 (2003), pp. 639–659.
[46] P. Zhang, R.-X. Liu, S.C. Wong, and S.Q. Dai, *Hyperbolicity and kinematic waves of a class of multi-population partial differential equations*, Eur. J. Appl. Math., 17 (2006), pp. 171–200.
[47] P. Zhang, S.C. Wong, and C.-W. Shu, *A weighted essentially non-oscillatory numerical scheme for a multi-class traffic flow model on an inhomogeneous highway*, J. Comput. Phys., 212 (2006), pp. 739–756.